สัญญาเลขที่ MRG5480123

รายงานวิจัยฉบับสมบูรณ์

การศึกษาการเกิดโครงสร้าง G-quadruplex จาก G-rich sequence ของ promoter regions

ผู้ช่วยศาสตราจารย์ เภสัชกร ดร.บดินทร์ ติวสุวรรณ
ภาควิชาอาหารและเภสัชเคมี คณะเภสัชศาสตร์
จุฬาลงกรณ์มหาวิทยาลัย

สนับสนุนโดยสำนักงานกองทุนสนับสนุนการวิจัย

Table of Contents

Abstract

Project code: MRG5480123

Project title: Study the Formation of G-quadruplex structures from G-rich sequence DNA on the promoter regions

Investigator: Bodin Tuesuwan, Asst. Prof., Ph.D., R.Ph., Department of Food and Pharmaceutical Chemistry, Faculty of Pharmaceutical Sciences, Chulalongkorn University

E-mail address: btuesuwan@pharm.chula.ac.th

Project period: 15 June 2011 – 10 April 2014

Abstract: This research mainly investigate the formation of G-quadruplex motifs adopted by G-rich sequences in the promoter region of CDKN2A tumor suppressor gene and of NF-KB1proto-oncogene. Spectroscopy techniques were conducted to demonstrate the formation of a stable mixed parallel/antiparallel G-quadruplex structure in both genes. Moreover, the G-quadruplex structure adopted by CDKN2A was further characterized by DMS footprinting experiments to reveal a stack of three G-tetrads. The competition experiments between duplex and G-quadruplex formation suggested that G-quadruplex structures could be presented under specified conditions, even in the presence of the C-rich complementary strand. By using CD spectroscopy, interestingly, various distinct phenomena were observes, including induction, destabilization, and topological change, with 5,10,15,20-tetrakis(*N*-methylpyridinium-4-yl)-21H,23H-porphyrin (TMPyP4) and *N*-methyl mesoporphyrin (NMM). These results provide the evidence for G-quadruplex formation within the promoter region of CDKN2A tumor suppressor gene and of

NF-KB1proto-oncogene *in vitro*, which could potentially play a role as a transcriptional regulator of this gene, and could also be manipulated by small molecules.

Keywords: G-quadruplex, CD Spectroscopy, Tumor suppressor gene, G-rich sequence

บทคัดย่อ

รหัสโครงการ: MRG5480123

ชื่อโครงการ: การศึกษาการเกิดโครงสร้าง G-quadruplex จาก G-rich sequence ของ promoter regions

ชื่อนักวิจัย: ผู้ช่วยศาสตราจารย์ เภสัชกร ดร.บดินทร์ ติวสุวรรณ ภาควิชาอาหารและเภสัชเคมี คณะเภสัชศาสตร์ จุฬาลงกรณ์มหาวิทยาลัย

E-mail address: btuesuwan@pharm.chula.ac.th

ระยะเวลาโครงการ: 15 มิถุนายน 2554 – 10 เมษายน 2557

บทคัดย่อ: งานวิจัยนี้ศึกษาการเกิดโครงสร้างจีควอดตรูเพร็ก (G-quadruplex) จากบริเวณโปรโมเตอร์ของยีน CDKN2A และ NF-KB1 โดยอาศัยเทคนิคทางสเปกโตสโคปี ยีนทั้งสองสามารถเกิดโครงสร้าง G-quadruplex ชนิดผสมระหว่าง parallel / antiparallel จากเทคนิค DMS footprinting ทำให้ทราบว่าโครงสร้าง G-quadruplex จากลำดับในบริเวณ โปรโมเตอร์ของ CDKN2A เป็น G-tetrad ซ้อนกัน 3 ชั้น และพบว่า แม้ในสภาวะที่มี C-rich complementary DNA อยู่ ก็ยังสามารถเกิดโครงสร้าง G-quadruplex ได้ นอกจากนี้สารกลุ่ม porphyrin บางชนิดสามารถเหนี่ยวนำให้เกิดโครงสร้าง G-quadruplex ได้หรือทำให้ conformation ของ G-quadruplex เปลี่ยนแปลงไป จากผลดังกล่าวแสดงให้เห็นว่า บริเวณของโปรโมเตอร์ของยีน CDKN2A และ NF-KB1 สามารถเกิดเป็นโครงสร้าง G-quadruplex ได้ และน่าจะมีบทบาทในกระบวนการควบคุมการแสดงออกของยีนและยังสามารถควบคุมโครงสร้าง G-quadruplex นี้ด้วยสารเคมี

คำหลัก: G-quadruplex, CD Spectroscopy, Tumor suppressor gene, G-rich sequence

Executive Summary

โครงการวิจัย: Study the Formation of G-quadruplex structures from G-rich sequence DNA on the promoter regions

วัตถุประสงค์

- To study whether G-rich sequences in the promoter of proto-oncogene (e.g., CDKN2) or tumor suppressor gene (e.g., NF-ΚB1) can adopt G-quadruplex structures.
- To determine topology (secondary structure) of G-rich sequences in the aqueous condition.
- To study the behavior and effects of small molecules on G-quadruplex DNA.

การดำเนินงานวิจัย

We explore the G-rich sequence on the promote region of proto-oncogene and of tumor suppressor gene. In this process, we perform some of searching a G-rich sequence for our experiment. We have selected the part of promoter region of CDKN2A (a proto-oncogene) and the part of promoter region of NF-ΚB1 (a tumor suppressor gene). The combination of biophysical analytical methods was used to investigate the G-quadruplex formation, its thermal stability and behavior. Then, the effects of G-quadruplex interacting agents, such as TMPyP4, NMM, and protoporphyrin IX, on G-quadruplex induction and stabilization were demonstrated. The binding stoichiometry and binding constant of

TMPyP4 to the G-quadruplex structures formed were determined by using UV-absorption titration experiments. Finally, the effect of pH and potassium salt on G-quadruplex formation was investigated.

ผลงานวิจัย

In our study, we demonstrate that the G-rich sequences in the promoter regions of CDKN2A tumor suppressor gene and NF-ĸB1 proto-oncogene have ability to form stable mixed parallel/antiparallel G-quadruplex structures. The mixed parallel/antiparallel G-quadruplex structure from CDKN2A is comprised of five-base, two-base, and three-base loops adopted by CDKN2A in the presence of KCl. The stable G-quadruplex structures form within the promoter regions of either NF-ĸB1 proto-oncogene or CDKN2A tumor suppressor gene may play an important biological role in gene regulation.

Moreover, we show that two G-quadruplex interacting agents, TMPyP4 and NMM displayed various effects, including induction, destabilization, topological change, on the G-quadruplex structures. The results for CDKN2A reveal stoichiometry constants of 1.76 and 1.94 with the apparent binding affinity constants of 2.50×10^{9} and 2.16×10^{6} M^{-1}, whereas the values for NF-ĸB1 were 1.57 and 3.56 with the apparent binding affinity constants of 1.14×10^{10} and 2.81×10^{6} M^{-1}. Ultimately, the competition experiments between duplex- and G-quadruplex or i-motif formation of CDKN2A gene suggested that G-quadruplex formation could present under certain conditions, even in the presence of the C-rich complementary strand, which can hybridize with the G-rich strand to form a stable Watson-Crick double helix.

Study the Formation of G-quadruplex structures from G-rich sequence DNA on the promoter regions

Introduction

Guanine-rich sequences throughout the genome may form unusual, stable structures called *G-quadruplex.* The most obvious of these guanine-rich sequences is at the telomere. Telomeres maintain the integrity of the chromosome end and represent a means of controlling the cellular lifespan.[1] Besides telomeric DNA, other guanine-rich regions include a number of gene promoters [2,3] which are also capable of forming G-quadruplex structures. It is believed that there is a correlation between G-quadruplex structure and gene function and genetic stability.[4,5] The discovery of an increasing number of proteins that interact with G-quadruplex structures and the possibility of a biological role for G-quadruplex DNA offers a novel avenue for targeted drug discovery. In addition to targeting these DNA structures with G-quadruplex interactive agents, other avenues include designing molecules that interact with G-quadruplex binding/interacting proteins.

Putative quadruplex sequences are predicted throughout the human genome (besides telomeres), more than three hundred thousand potential quadruplexes could exist.[6] Moreover, it was reported that the promoter regions (in both sense and antisense strand) are significantly enriched in G-quadruplex motif [7] and was proposed that G-quadruplex might be involved in gene regulation. Also, it has been show the correlation between G-quadruplex formation and genetic stability. Therefore, G-quadruplex motifs on the promoter regions may correlate with carcinogenesis. However, the molecular mechanisms that contribute mutations are never clearly understood.

The intent of our project is studying the possibility of forming structure of G-quadruplex DNA arising from the variation of G-rich sequences on the promoter of tumor suppressor gene and proto-oncogene. Also, we look for the small molecules that can bind and stabilize G-quadruplex-forming structures which might be used for further gene expression study and design better G-quadruplex interactive molecules. This study would bring us a tool for further understanding of existing G-quadruplex structure on the promoter on tumor suppressor gene/proto-oncogene and steering to control gene expression via G-quadruplex motif. If we could manipulate the expression on tumor suppressor gene/proto-oncogene, we may battle the cancer and several genetic disorders via this approach. This work would extend the area of G-quadruplex DNA, one of the targets for cancer–drug discovery. Ultimately, the knowledge in the field of G-quadruplex interacting/stabilizing agents would facilitate the development the better compounds for the therapeutic uses.

Objectives

- To study whether G-rich sequences in the promoter of proto-oncogene (e.g., CDKN2) or tumor suppressor gene (e.g., NF-ΚB1) can adopt G-quadruplex structures.
- To determine topology (secondary structure) of G-rich sequences in the aqueous condition.
- To study the behavior and effects of small molecules on G-quadruplex DNA.

Literature Review

G-quadruplex structures consist of multiple stacked G-tetrads, which form from Hoogsteen hydrogen bonding between the N1, N7, O6, and N2 of guanine bases (Figure 1).

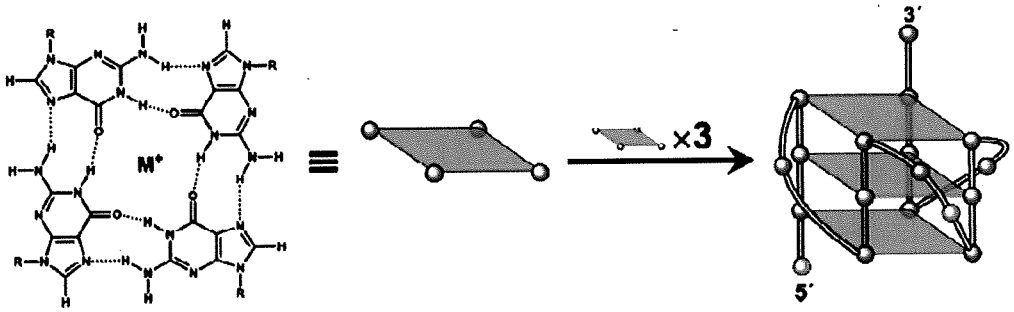

Figure 1 Structure of a G-tetrad and an example of the folding pattern of a known intramolecular G-quadruplex structure in c-MYC promoter region.[8]

Although stabilized by extensive hydrogen bonding, such orientation of guanine bases to form a G-tetrad results in strong negative electrostatic potential created by guanine O6 oxygen atoms. Therefore, metal ions are generally assist the formation and stabilization of G-quadruplex structures, especially alkali metals, such as Na^+ and K^+. These ions are located in the interior channel formed at the core of each G-tetrad and coordinated with O6 atoms of the guanines in adjacent G-tetrads [9] to neutralize the above-mentioned strong negative electrostatic potential created by these guanine O6 oxygen atoms.[10]

G-quadruplex arrangements could be categorized in three classes: a) tetramolecular G-quadruplex (Figure 2b) which is constructed from four separate strands, each of which consists of at least one G-tract, b) bimolecular G-quadruplex (Figure 2c) which is constructed from two strands, each normally having two G-tracts, c) monomolecular, also called as intramolecular, G-quadruplex (Figure 2d) which is normally constructed from four

consecutive G-tracts. If there are more than four G-tracts, many distinct G-quadruplex structures can be formed, often in equilibrium with one another.[9] Furthermore, G-quadruplex structures could be classified based on their strand polarities and the locations of the loops which connect the guanine strands to form either bimolecular or intramolecular G-quadruplex structures.[11] Class of Parallel G-quadruplex structures is defined when all strands are in parallel alignment and have connecting loops to link the top G-tetrad with the bottom G-tetrad, which are called as propeller loops (other termed chain-reversal loops or external loops) (Figure 2a). Secondly, G-quadruplex structures are indicated as anti-parallel when at least one of the four strands is in an opposite direction to the others. Two other types of loops are observed in these structures. Lateral (also termed as edge-wise) loops link adjacent G-strands (Figure 2b), and can be located either on the same or opposite faces of a G-quadruplex structure. Another type of anti-parallel loops is the diagonal loops, which connect opposite G-strands (Figure 2b).

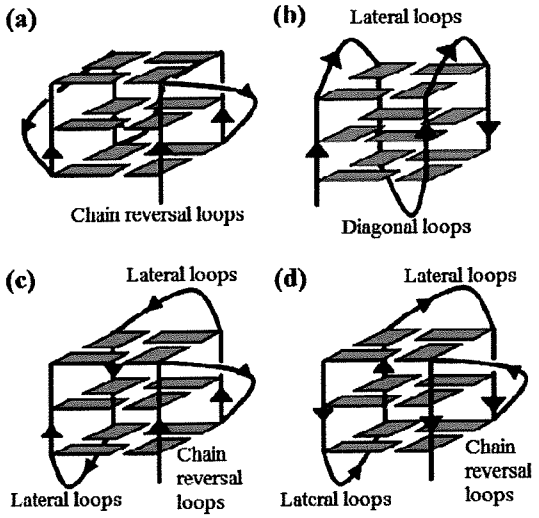

Figure 2 Structures of (a) a parallel G-quadruplex structure with chain reversal loops, (b) an anti-parallel G-quadruplex structure with a diagonal loop and two lateral loops, (c) a hybrid [3+1] anti-parallel G-quadruplex structure with two lateral loops and a chain reversal loop, and (d) another hybrid [3+1] anti-parallel G-quadruplex structure with two lateral loops and a chain reversal loop.[9]

Although G-quadruplex structures can obviously be adopted *in vitro* by G-rich DNA in the presence of either Na^+ or K^+, G-quadruplex formation might not occur *in vivo*. However, there is the discovery of various G-quadruplex-interacting proteins. For example, the repressor/activator protein 1 (RAP1) from yeasts and the β-subunit of the *Oxytricha* telomere binding protein have been shown to not only bind to G-quadruplex structures, but also facilitate G-quadruplex formation.[12,13] On the other hand, helicases, such as Simian virus (SV) 40 large T-antigen, Bloom's syndrome helicase (BLM), Sg1 helicase (*Saccharomyces cerevisiae* homologue of BLM) from yeasts, and Werner syndrome helicase from humans have been found to unwind G-quadruplex structures.[14,15,16,17] These cellular mechanisms for removing G-quadruplexes suggest that G-quadruplex formation must occur within cells. Besides the G-quadruplex formation found within telomeres, it has

been discovered within the promoter regions of genes, acting as transcriptional regulators.[18]

Telomeres are located at the end of chromosomes. They contain a short single-stranded 3′ overhang, which comprises 5′-TTAGGG-3′ tandem repeats. This overhang is essential for cell survival because shortened telomeres could cause genomic instability and lead to cell senescence.[19] Immortal and/or rapidly dividing cells, such as germ cells, inflammatory cells, and tumor or cancer cells,[20] the telomere length can be maintained by telomerase, which is a reverse transcriptase enzyme that adds TTAGGG sequence repeats to telomeres. In contrast, telomerase is normally not found in normal somatic cells.

Since the discovery of G-quadruplex formation within the promoter region of the c-MYC proto-oncogene,[21] there have been extensive interests in such process within the promoter regions of genes, especially proto-oncogenes, such as c-MYC, VEGF, HIF-1α, RET, KRAS, c-kit, bcl-2, PDGF-A, and c-myb. These have stirred researchers to believe that G-quadruplex structures found within the promoter regions of genes might play a role in the regulation of gene expression. One of several examples is cationic porphyrin TMPyP4, a G-quadruplex-interacting compound, could down-regulate c-MYC expression *in vivo*.[22] Moreover, Balasubramanian et al. suggested that molecular crowding, which is the condition that mimics high concentrations of macromolecules in the nucleus, may stabilize the formed G-quadruplex structures, and the negative superhelicity originated from transcription may be another dynamic force for G-quadruplex formation.[13] Nevertheless, it was still unclear how G-quadruplex structures could compete with duplex

DNA even though GC-rich sequences are actually more stable, as indicated by higher melting temperatures than those of AT-rich sequences.

Due to the emergence of G-quadruplex structures as an attractive target for anti-cancer drug design, several research groups have attempted to identify small organic compounds that interact with G-quadruplex structures. To date, several classes of compounds have been reported, for instances, TMPyP4 (a cationic porphyrin), telomestatin, BSU1051 (a 2,6-diamido anthraquinone derivative), RHPS4, (a pentacyclic quinoacridinium salt), BRACO-19, (a tri-substituted acridine derivative).

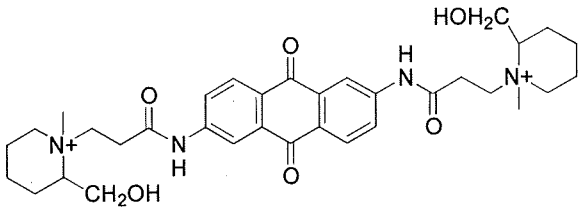

BSU-1051

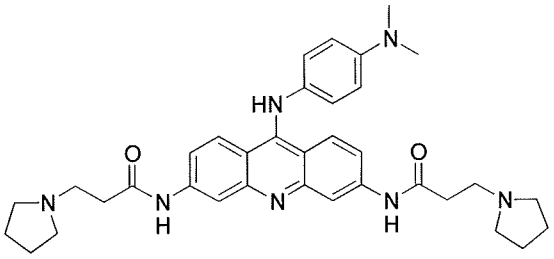

BRACO-19

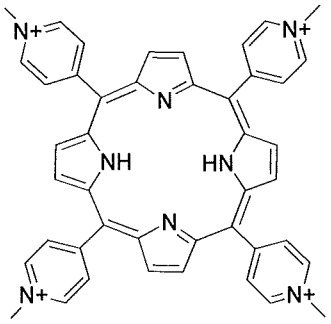

TMPyP4

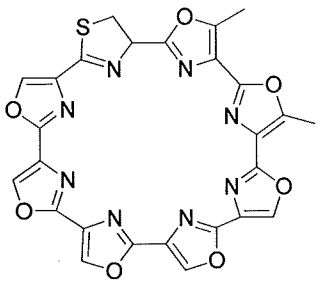

Telomestatin

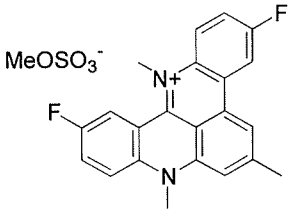

RHPS4

Figure 3 Examples of G-quadruplex-interactive ligands

Materials and Methods

The structure of the G-quadruplex formed in each oligonucleotide was characterized using a combination of CD spectroscopy and gel electrophoresis, along with DMS footprinting. Furthermore, thermal stability was investigated using CD spectroscopy to determine the melting temperature (T_m). Then, the effects of G-quadruplex interacting agents, such as TMPyP4, NMM, and protoporphyrin IX, on G-quadruplex induction and stabilization were demonstrated. The binding stoichiometry and binding constant of TMPyP4 to the G-quadruplex structures formed were determined by using UV-absorption titration experiments. Finally, the effect of pH and potassium salt on G-quadruplex formation was investigated.

DNA oligonucleotides derived from the promoter regions of NF-KB1 and CDKN2A genes (HPLC-purified) were purchased from Sigma-Aldrich Co., Ltd. (Singapore), whereas Telomere22 (Tel22) (high affinity purification(HAP)-purified) and comp-CDKN2A (PAGE-purified) were purchased from Pacific Science Co., Ltd. (Bangkok, Thailand). All DNA oligonucleotides were used without further purification. The stock solutions of each DNA oligonucleotide were prepared in 1XTE buffer (100 mM Tris-HCl and 10 mM EDTA) at pH 7.4. The oligonucleotide concentrations (ng/μL) were determined using a micro-volume UV-visible spectrophotometer, NanoDrop 2000 (Thermo Scientific, Wilmington, DE, USA), and subsequently converted to μM using their molecular weight obtained from the suppliers.

Table 1 Sequences of the oligonucleotides used in this study

Name	Sequence (5' to 3')
Tel22	AGG GTT AGG GTT AGG GTT AGG G
NF-KB1	GGG GCC GCT TCG GGG CGC CGG GCG AGG GG
CDKN2A	GGG CAG CTG GGA GGG GAA TGG G
comp-CDKN2A	CCC ATT CCC CTC CCA GCT GCC C

G-quadruplex formation

Each oligonucleotide was dissolved in an appropriate buffer, which was 1XTE in the absence of salt or 1XTE in the presence of either 100 mM NaCl or 100 mM KCl. Then, each solution was divided into three, which were treated as follows: a) sample 1 (No heat) was measured immediately without heating, b) sample 2 (Immediately cooled) was heated at 95°C for 5 min, then immediately cooled down on an ice bath, and c) sample 3 (Slowly cooled) was heated at 95°C for 5 min, then gently cooled down to room temperature. The appropriate condition was selected and used throughout all experiments.

G-quadruplex formation was monitored using circular dichroism spectroscopy. CD spectra were recorded on a JASCO J-815 spectrophotometer (Jasco Corporation, Tokyo, Japan) equipped with a temperature control system. The DNA oligonucleotide concentration used in all CD experiments was 10 μM. For each sample, the CD spectrum obtained was an average of three repeated scans at 25°C. Each spectrum was smoothened and subtracted by the CD spectrum corresponding to medium.

Thermal stability of G-quadruplex structures

CD spectroscopy was used to determine the melting temperature (T_m) by monitoring a change of ellipticity at either 295 or 260 nm as the temperature was ramped up from 5 to 95°C at a rate of 1°C/min for mixed parallel/antiparallel and parallel G-quadruplex structures, respectively.

Structural characterization of G-quadruplex structures by DMS footprinting

5'- radiolabeled CDKN2A oligonucleotide was incubated under the optimum conditions for G-quadruplex formation. The 5'- radiolabeled G-quadruplex DNA were purified by a non-denaturing PAGE. DMS methylation on 5'- radiolabeled G-quadruplex DNA was allowed for 5, 10, 20, 30, and 40 min at room temperature. The reaction was stopped and precipitated. The oligonucleotide pellet was subjected to heat treatment with 10% piperidine at 95 °C for 15 min. The samples were then dissolved in formamide loading dye and analyzed by 10% denaturing PAGE. The images were visualized by PhosphoImager.

Effects of G-quadruplex interacting agents on G-quadruplex induction and stabilization

The effects of known G-quadruplex interacting agents, which are TMPyP4, NMM, and protoporphyrin IX, were investigated. Induction of G-quadruplex formation by ligands was monitored by the change in CD spectra after the incubation of each oligonucleotide with 3 molar equivalents of ligand for 1 min. If there is any inducing effects, then thermal stability

of induced G-quadruplex structure would be determined. For the G-quadruplex interacting compounds with no inducing effect, their stabilizing effects were demonstrated.

UV-Visible absorption titration

Absorption spectra were measured on an Agilent 8453 UV-vis spectrophotometer. UV-vis absorption titrations were carried out by stepwise additions of the G-quadruplex solution in 1XTE buffer containing 100 mM KCl to a cell containing ligand and absorption spectra were recorded in the range of 350-500 nm at room temperature. The titration was terminated when the wavelength and intensity of the absorption band for ligand no longer changed upon three successive additions of the G-quadruplex solution. For data analysis, Scatchard plots were constructed between r n $/C_f$ against r using Equation 1, as well as r versus C_f using Equation 2, where r is the number of ligand molecules bound per mole of quadruplex (C_b/C_{DNA}), C_f is the free ligand concentration (μM), n is the number of equivalent binding sites, and K_a is the ligand affinity for those sites. The concentration of free ligand (C_f) and bound ligand (C_b) were calculated using $C_f = C_T(1-\alpha)$ and $C_b = C_T - C_f$, respectively, where C_T is the total ligand concentration. The fraction of bound ligand (α) was calculated using the equation $\alpha = (A_f - A)/(A_f - A_b)$, where A_f and A_b are the absorbance of free and fully bound ligand at the Soret maxima of ligand, respectively, and A is the absorbance at the Soret maxima at any given point during the titration.

$$\frac{r}{C_f} = nK_a - K_a r \quad (1)$$

$$r = \frac{n_1 K_{a1} C_f}{1 + K_{a1} C_f} + \frac{n_2 K_{a2} C_f}{1 + K_{a2} C_f} \quad (2)$$

As the Scatchard analysis using Equation 2 was nonlinear regression method was employed to evaluate the binding parameters according to Equation 3.

$$r = \frac{n_1 C_f}{K_{d1} + C_f} + \frac{n_2 C_f}{K_{d2} + C_f} \quad (3)$$

SigmaPlot® was used for all fitting analyses. The percent hypochromicity of the Soret band of TMPyP4 was calculated using the percent hypochromicity = $[(\varepsilon_f - \varepsilon_b)/\varepsilon_f] \times 100$, where $\varepsilon_b = A_b/C_b$ and $\varepsilon_f = A_f/C_f$.

Competition between duplex- and G-quadruplex or i-motif formation

In general, promoter regions of genes consist of two complementary strands which hybridize to form a Watson-Crick double-helix under standard conditions.[23] However, the double-helices formed in the promoter regions containing G-rich and C-rich complementary strands can be disrupted, as a result of the G-quadruplex formation by the G-rich strand and/or i-motif formation by the complementary C-rich strand.[24] The stable G-quadruplex structures could be formed in the presence of potassium ions, while i-motif structures could be formed under acidic conditions. Therefore, either the acidic pH and/or the presence of potassium ions may motivate a transition from duplex- to G-quadruplex or i-motif formation within G-rich regions. Herein, a competition between duplex- and either G-quadruplex or i-motif formation within promoter region of CDKN2A was studied.

Two complementary strands of CDKN2A were mixed at a concentration of 100 μM for each strand (1:1 molar ratio). Afterwards, the mixture was heated and then slowly cooled

to room temperature, allowing two complementary strands to form a Watson-Crick double helix. The duplex was diluted to 10 μM of each strand with 1XTE (pH 7.4). Various conditions were applied for inducing structural conversions, such as addition of 100 mM KCl, decreasing the pH to 4.0 by adding HCl, as well as simultaneous addition of 100 mM KCl and decreasing the pH to 4.0. After applying appropriate conditions, each sample was incubated at 37°C and slightly shaken for 5 h, allowing the structural transformation. The structural transformation was monitored using circular dichroism spectroscopy. In addition, the melting temperatures of the resulting structures were also determined using circular dichroism spectroscopy.

Results and Discussion

Optimization of conditions for G-quadruplex formation

In this study, this procedure was first verified G-quadruplex formation. To optimize the conditions to be used for G-quadruplex formation in all experiments, samples of each oligonucleotide containing no salts, 100 mM NaCl, or 100 mM KCl were prepared and incubated with or without heating, followed by cooling down at two different rates. The resulting CD patterns were then compared.

Noticeably, CDKN2A both in the absence and presence of salts exhibited distinct CD patterns when different incubation methods, with and without heating, were used (Figure 4a). For instance, without heating, the CD spectrum of CDKN2A in the absence of salts exhibited three characteristic peaks with two positive peaks at 214 and 262 nm and a negative peak at 245 nm (Figure 4a, blue line). In contrast, when incubated with heating, the resulting CD spectra exhibited the same negative peak at 245 nm, but the two positive peaks were shifted to 215 nm and 255 nm, whereas the peak intensities were also changed (Figure 4a, green and red lines). In addition, this trend was also observed with CDKN2A in the presence of either 100 mM NaCl or KCl. For NF-κB1 and Tel22, the CD spectra obtained from different incubation methods showed similar patterns with characteristic peaks at the same positions, but with slightly different intensities (Figure 4b, c).

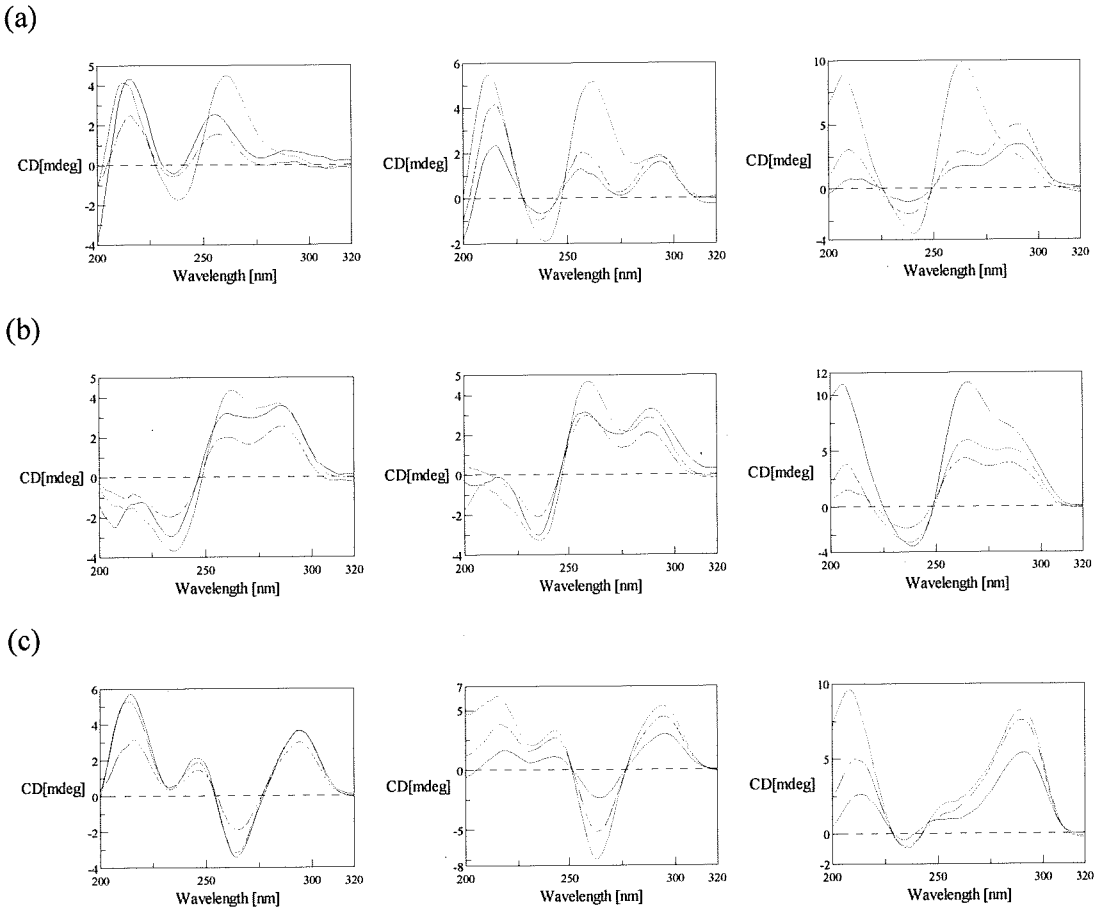

Figure 4 CD spectra of G-rich DNA oligonucleotides derived from (a) CDKN2A, (b) NF-κB1, and (c) Tel22 in the absence of salts (left) and presence of either 100 mM NaCl (middle) or 100 mM KCl (right). The overlayed spectra were obtained from various incubation methods, which are no heat (blue line), heating with immediate cooling (green line), and heating with slow cooling (red line).

Although both cooling rates, could provide quite similar CD patterns, the latter was selected because the slow cooling process can yield canonical quadruplex structures, which are thermodynamically stable, as suggested by Bardin and Leroy.[25] In this study, heating with slow cooling down to room temperature overnight was used as an incubation method in all experiments to obtain the canonical G-quadruplex structures with thermodynamic stability.

G-quadruplex structure characterization by circular dichroism

CD spectroscopy technique has been extensively used to provide primary evidence for the G-quadruplex structures. In addition, there is much currently available information of signature CD spectra for several well-defined solution structures of G-quadruplex.

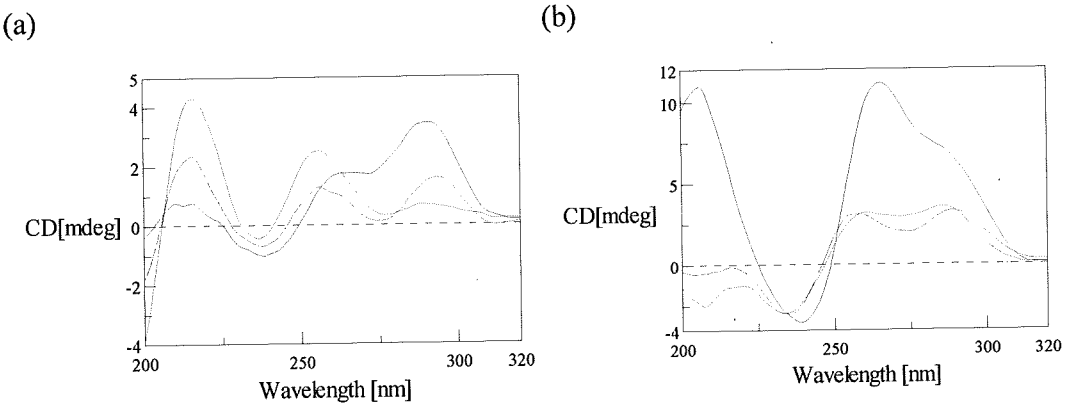

Figure 5 CD spectra of G-rich DNA oligonucleotides derived from (a) CDKN2A and (b) NF-KB1 genes in the absence of salts (blue line) and presence of either 100 mM NaCl (green line) or 100 mM KCl (red line).

As shown in Figure 5a, the CD spectrum of CDKN2A in the absence of salts (blue line), exhibited a maximum positive peak at 257 nm and a negative peak at 236 nm, which are characteristics of unstructured oligonucleotides.[26] In contrast, when exposed to salts, the obtained CD patterns indicated the formation of G-quadruplex structures. In the presence of 100 mM NaCl, the CD spectrum of CDKN2A (green line) demonstrated two positive peaks near 260 and 290 nm and a negative peak near 240 nm, all of which are the characteristic signature of a mixed parallel/antiparallel G-quadruplex structure.[27] Similarly, CDKN2A in the presence of 100 mM KCl exhibited the CD spectrum with three characteristic peaks corresponding to a mixed parallel/antiparallel G-quadruplex structure.

These results indicated that monovalent cations are required to induce G-quadruplex formation in CDKN2A.

For NF-KB1, Figure 5b shows that it could adopt the G-quadruplex structures both in the absence of salts and also in the presence of either 100 mM NaCl or 100 mM KCl. All CD spectra exhibited two positive peaks around 260 and 290 nm and a negative peak around 240 nm, which are characteristics of a mixed parallel/antiparallel G-quadruplex structure.[27]

The previously reported G-quadruplex structures along with G-quadruplex forming sequences revealed that G-rich sequences with two single-nucleotide loops have been found within the promoter regions of human genes with high occurrence, and such sequences have a predisposition towards a parallel topology. In contrast, bcl-2 promoter sequence containing only one single-nucleotide loop at the 3' end adopted distinct topology, which is a mixed parallel/antiparallel G-quadruplex structure. The G-rich sequence of CDKN2A has a propensity to form G-quadruplex structures with a possible single-nucleotide loop similar to that found in bcl-2 promoter sequence. Even though the single-nucleotide loop within CDKN2A is located at central loop, rather than the 3' end loop found in bcl-2, the results suggested that a mixed parallel/antiparallel G-quadruplex structure was also formed in G-rich CDKN2A in the presence of either 100 mM NaCl or KCl. In addition, such sequences have been found not only in the promoter regions of genes, but also in 3'-untranslated regions (UTR), like in STAT3 gene. Therefore, our results obtained with CDKN2A could also serve as additional evidence to suggest that G-rich sequences containing a single-nucleotide loop tend to adopt a mixed

parallel/antiparallel G-quadruplex structure, regardless of the location of the single-nucleotide loop.

In the case of NF-ΚB1, the G-quadruplex topology was formed with three loops of varying lengths, which exhibit obvious sequence similarity to HRAS-1 (GGG TTG CGGCGCA GGG CAC GGG).[28] However, HRAS-1 adopted an anti-parallel G-quadruplex structure, while NF-ΚB1 adopted mixed parallel/antiparallel topology. It is very interesting that G-quadruplex structures containing loops of varying lengths can be found in various regions of genes, such as in human promoter regions (HAS-1, Rb), 5'-UTR (human estrogen receptor α), 3'-UTR (STAT3), and also in the promoter regions of parasite genes (*Plasmodium falciparum var*). Such G-rich sequences can form not only anti-parallel G-quadruplex structures like in HRAS-1 and Rb but also mixed parallel/antiparallel G-quadruplex structures which have been reported for human estrogen receptor α, STAT3, and *Plasmodium falciparum var* gene. The preference for mixed parallel/antiparallel G-quadruplex formation within NF-ΚB1 may be explained by the length of G-tracts as it has been suggested that the "3+1" scaffold found in mixed parallel/antiparallel topology is the most stable geometry of the G-quadruplex core built from G-tracts containing three guanines (G3-tracts).[29] In addition, the G-quadruplex structure found within NF-ΚB1 is noticeably the first discovery of mixed parallel/antiparallel G-quadruplex structures adopted by the G-rich sequences with loops of varying lengths in the promoter regions of human genes.

Thermal stability of formed G-quadruplex structures

The melting temperatures were determined using the melting curves constructed from the CD ellipticity at 295 nm as a function of temperature. As shown in Figure 6, all the formed G-quadruplex structures exhibited a monophasic melting curve.

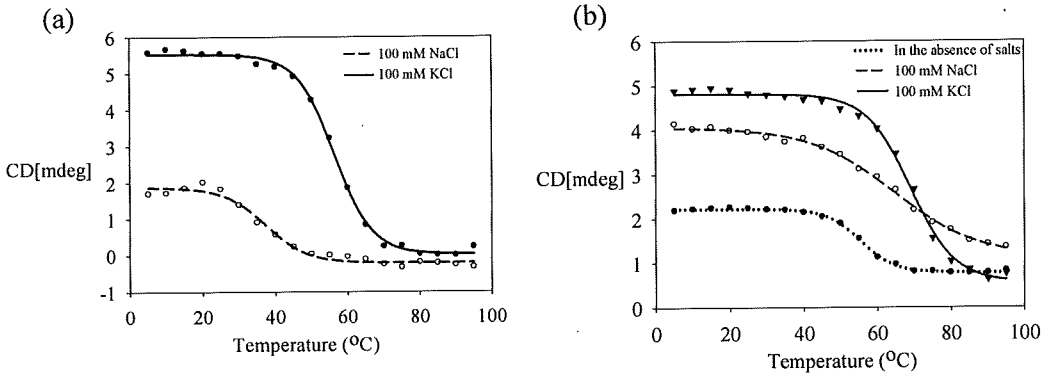

Figure 6 Melting curves of the G-quadruplex structures formed within the promoter regions of (a) CDKN2A and (b) NF-KB1 under the specified conditions.

Table 2 Melting temperatures of the G-quadruplex structures formed within promoter regions of CDKN2A and NF-KB1 genes.

Gene	Melting Temperature (°C)		
	No salt	100 mM NaCl	100 mM KCl
CDKN2A	-	37	56
NF-KB1	55	64	69

The G-quadruplex structures formed in both genes exhibited the highest melting temperature when 100 mM KCl was used to induce G-quadruplex formation. These results correspond with previous reports, which suggested that potassium has higher stabilizing power than sodium due to better coordination of potassium.[30] The difference in the thermal stability on both sequences may arise from the different lengths and

sequences of loops, which have been previously reported to play an important role in the overall folding and stability.[31] Under the same conditions, the G-quadruplex structure adopted by the G-rich sequence of NF-κB1 actually exhibited a higher melting temperature than that of the G-quadruplex structure adopted by CDKN2A.

The possible loops of NF-κB1 contain high prevalence of G and C bases, which may provide strong base-base stacking interactions within the loops and stacking of the loops onto G-quadruplex structures, leading to the high melting temperatures observed in this study.

Dimethyl Sulfate (DMS) footprinting

To gain further information on the formed G-quadruplex structures, DMS footprinting technique was applied to identify the guanine bases involved in the formation of G-tetrads in G-quadruplex structures.[32] Normally, the N7 position of guanine bases in duplex and single-stranded DNA is available for methylation by DMS. In contrast, this particular position of the guanine bases is involved in Hoogsteen hydrogen bonding to form G-tetrads in G-quadruplex structures, and thus, inaccessible for methylation by DMS.[33] In this study, the G-quadruplex structure adopted by CDKN2A in the presence of 100 mM KCl was investigated using this technique.

In order to determine the guanine bases involved in G-tetrad formation, the DMS footprint of single-stranded CDKN2A (ssCDKN2A) was compared with that obtained after G-quadruplex formation using 100 mM KCl (Figure 7a). The results showed that all the guanines in ssCDKN2A (lanes 6 and 11) were methylated by DMS leading to DNA cleavages, whereas several guanine bases in the G-quadruplex structure induced by 100

mM KCl (lanes 1-5 and 12-16) were protected from DMS methylation. The G-rich sequence within the CDKN2A promoter region has the propensity to form two plausible three-tetrad G-quadruplex structures depending on which G residues in the four-residue G-tract (G13-G16) that are involved in G-tetrad formation. According to the DMS footprint of G14-G16 were fully protected from methylation, while G13 was partially protected. Therefore, G13 should be assigned in the loop region and might not be involved in G-tetrad formation.

Theoretically, G1-G3, G9-G11, G14-G16 and G20-G22 in the three-tetrad G-quadruplex structure adopted by CDKN2A should be fully protected. In this study, the obtained DMS footprints (Figure 7a) showed full protection at G2-G3, G9-G11, G14-G16, and G20-G21, while the two terminal guanine bases at the 5' and 3' ends (G1 and G22, respectively) were methylated by DMS. However, pronounced cleavages of the two terminal guanines at the 5' and 3' ends of G-quadruplex structures have been commonly observed due to breathing of the conformation.[21] Based on these results, it is therefore not unusual to predict that CDKN2A adopted a three-tetrad G-quadruplex structure. When taking into account the results from both the CD and DMS footprinting experiments, an intramolecular mixed parallel/antiparallel G-quadruplex structure consisting of three G-tetrads, as well as five-base, two-base, and three-base loops, is proposed. As the topology of the loops cannot be predicted from either CD or DMS footprinting experiments, three plausible G-quadruplex topologies with distinct loop types and orientations are proposed in Figure 8.

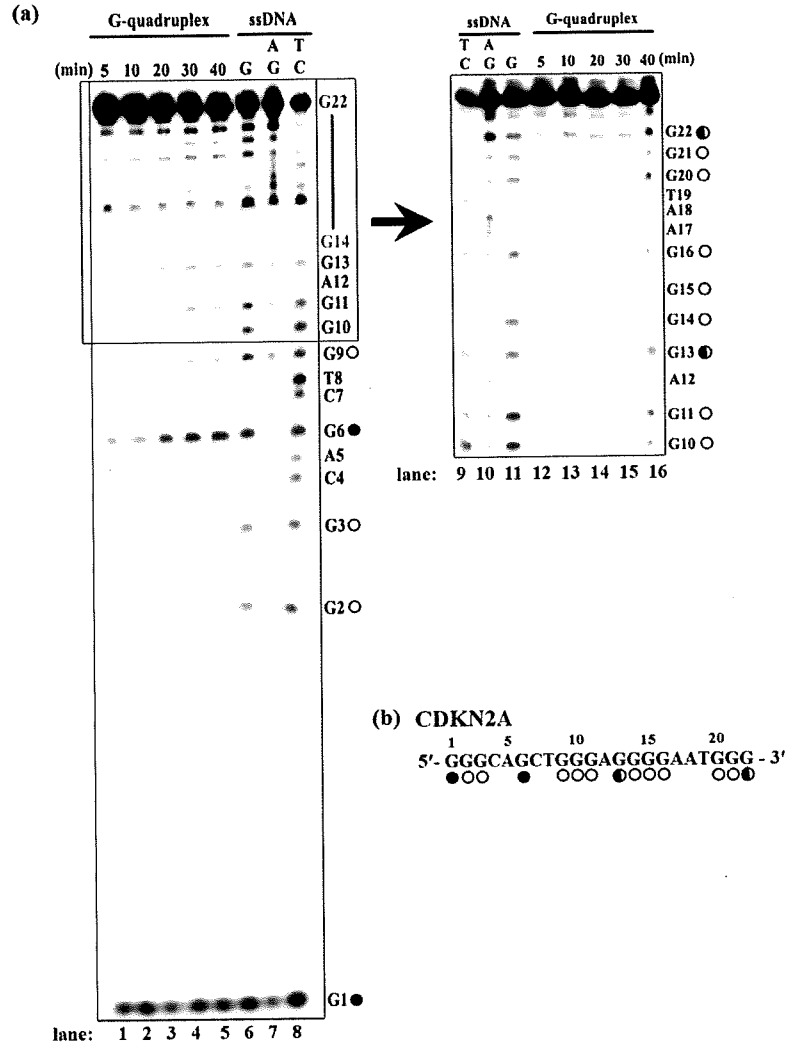

Figure 7 (a) DMS footprints of CDKN2A in either single-stranded DNA (ssDNA) state (lanes 6 and 11) or G-quadruplex structure adopted in the presence of 100 mM KCl after the treatment with DMS as a function of time (5, 10, 20, 30, and 40 min) (lanes 1-5 and 12-16). Lanes 7 and 10 show a purine sequencing reaction, whereas lanes 8 and 9 show a pyrimidine sequencing reaction. In the right panel were the same as those used to obtain the left panel, but the samples were loaded 30 min earlier, (b) G-rich sequence of CDKN2A with all the guanines labeled according to DMS methylation. The guanines fully protected from DMS methylation are indicated with open circles, whereas the partially protected ones are indicated with half-filled circles, and those with no protection are indicated with filled circles.

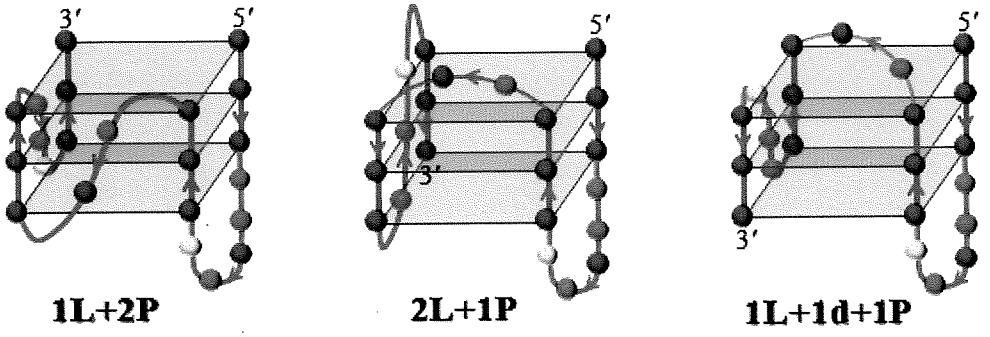

Figure 8 Proposed topologies for the mixed parallel/antiparallel, three-tetrad G-quadruplex structure adopted by CDKN2A. These topologies are distinguished by different existing loop types: (a) a lateral loop (L) and two chain reversal loops, also known as propeller loops (P), (b) two lateral loops and a chain reversal loop, (c) a lateral loop, a diagonal loop (d), and a chain reversal loop. Loop regions are shown as orange lines with the arrows indicating loop directions.

Effects of G-quadruplex interacting agents on the thermal stability of G-quadruplex structures

The effects of well known G-quadruplex interacting agents, such as TMPyP4 and NMM, as well as a porphyrin analogue, protoporphyrin IX (PP IX), on the thermal stability of G-quadruplex structures were examined on a basis of melting temperatures using CD spectroscopy. In addition, the CD spectra obtained before and after performing melting experiments were compared.

Figure 9 - Figure 17 show the effects of ligands on the G-quadruplex structures adopted by Tel22, CDKN2A, and NF-KB1 in the absence of salts and in the presence of either KCl or NaCl. The results obtained showed various distinct trends, which can be categorized into two main groups. The first group mainly includes NMM and protoporphyrin IX, the ligands that could not either induce (in the case of CDKN2A without

salts) or affect the formed G-quadruplex structures, whereas the second group primarily comprises TMPyP4, the ligand that could either induce or affect the formed G-quadruplex structures.

Minimal effects of NMM and protoporphyrin IX

For the first group, upon adding of 3 eq. of the ligand, the effects of each ligand on the G-quadruplex structures were not observed, as indicated by no change in the CD spectra either before or after conducting melting experiments. Additionally, the changes in the CD patterns during melting experiments were similar to those obtained in the absence of ligands, which are in agreement with a small difference in the melting temperatures (ΔT_m) by only 0-1°C compared with those obtained without ligands. Obviously, these results were observed in all the G-quadruplex structures in the presence of PP IX (column d in Figure 9 - Figure 17), suggesting that protoporphyrin IX did not have any effects on G-quadruplex structures. According to the report by Li et al.[34] PP IX specifically binds to parallel G-quadruplex structures. However, all the oligonucleotides used in this study adopted either anti-parallel or mixed parallel/antiparallel G-quadruplex structures, it is therefore not unexpected that PP IX could not interact with these G-quadruplex structures.

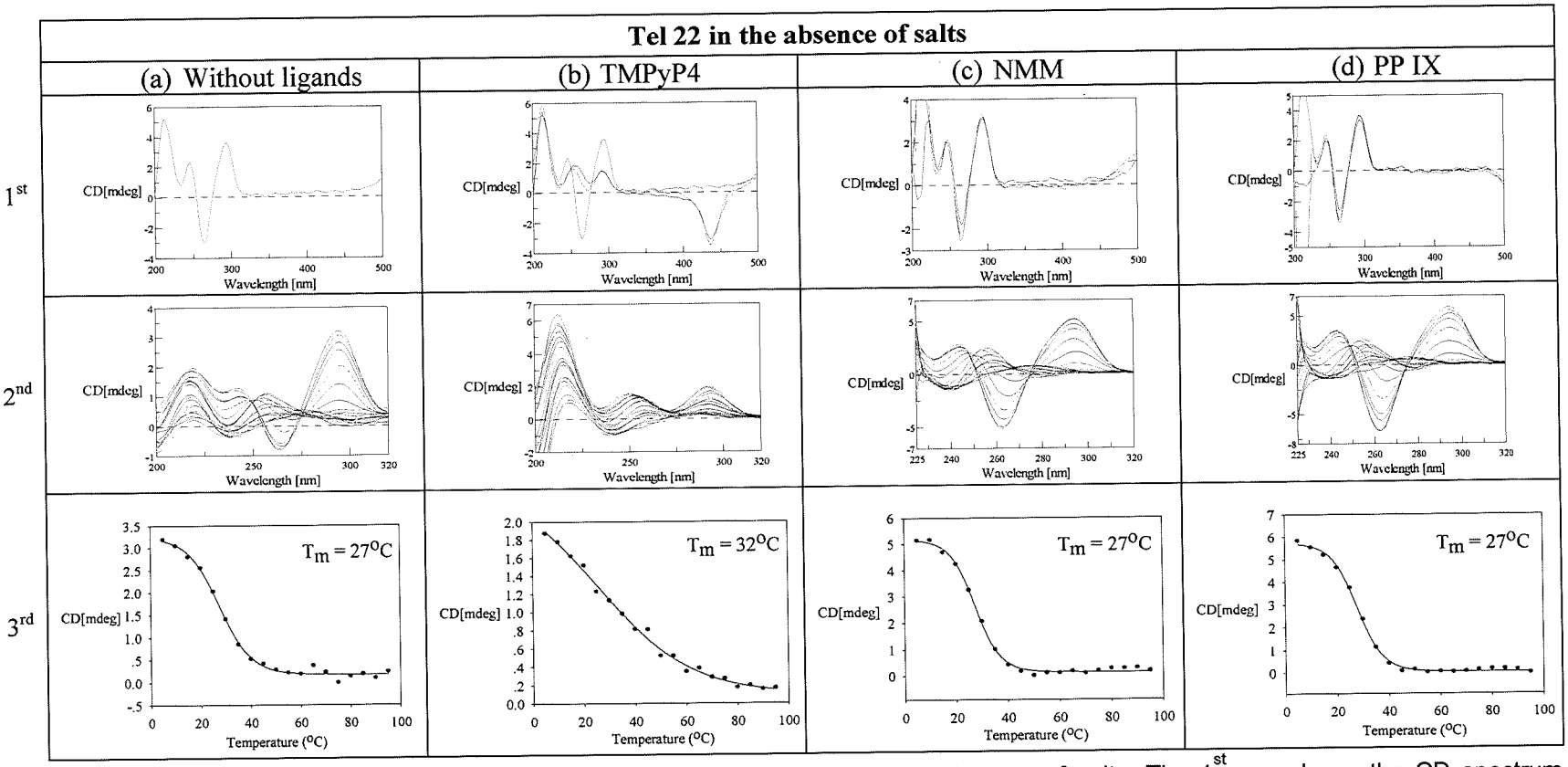

Figure 9 Effects of ligands on the G-quadruplex structure adopted by Tel22 in the absence of salts. The 1st row shows the CD spectrum of G-quadruplex without ligands (blue line) compared with those obtained in the presence of each ligand before and after T_m experiments (green and red lines, respectively). The 2nd row shows the CD spectra obtained at various temperatures (5-95°C) during T_m experiments. The last row shows the melting profiles in the absence or presence of each ligand (3 eq.) as indicated in the column heading.

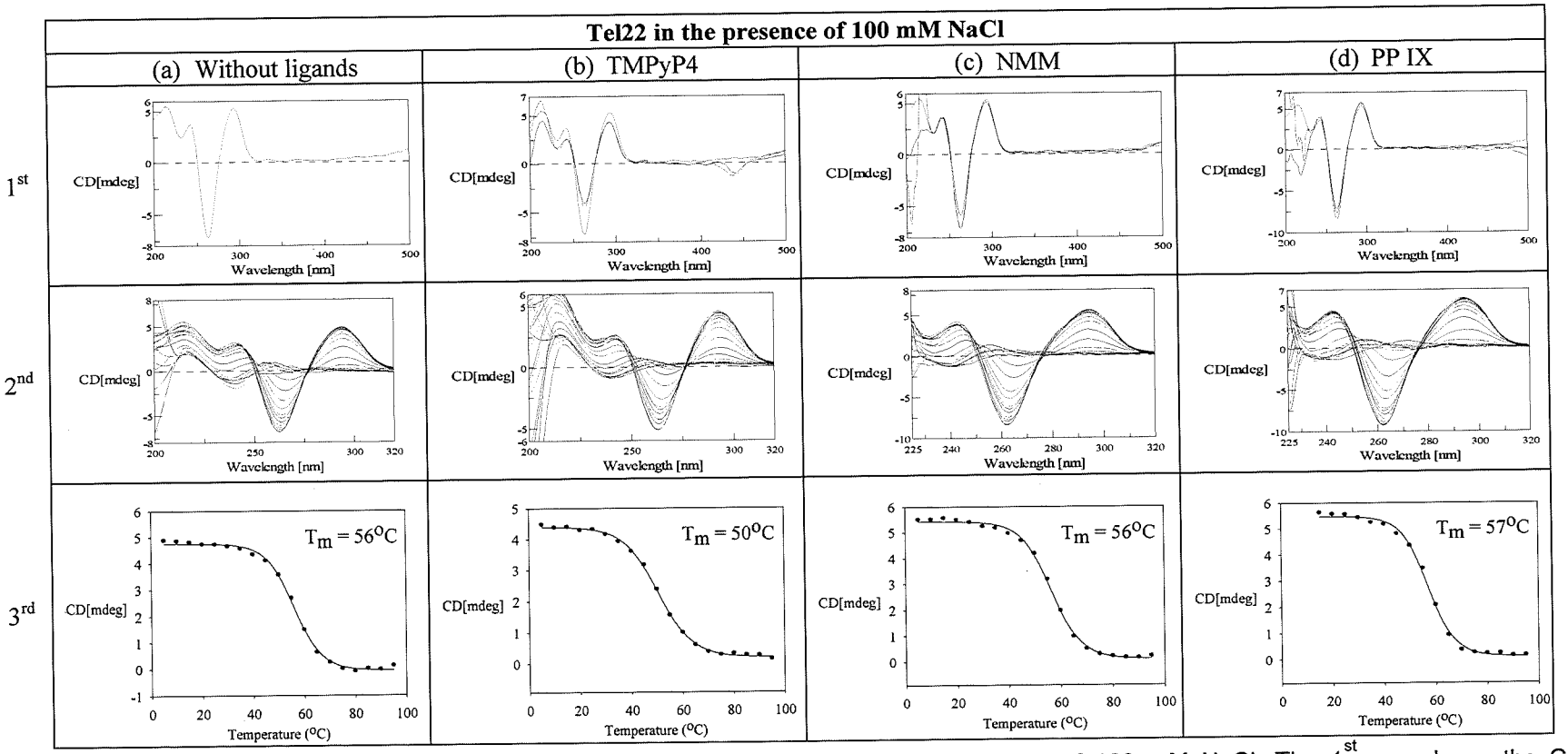

Figure 10 Effects of ligands on the G-quadruplex structure adopted by Tel22 in the presence of 100 mM NaCl. The 1st row shows the CD spectrum of G-quadruplex without ligands (blue line) compared with those obtained in the presence of each ligand before and after T_m experiments (green and red lines, respectively). The 2nd row shows the CD spectra obtained at various temperatures (5-95°C) during T_m experiments. The last row shows the melting profiles in the absence or presence of each ligand (3 eq.) as indicated in the column heading.

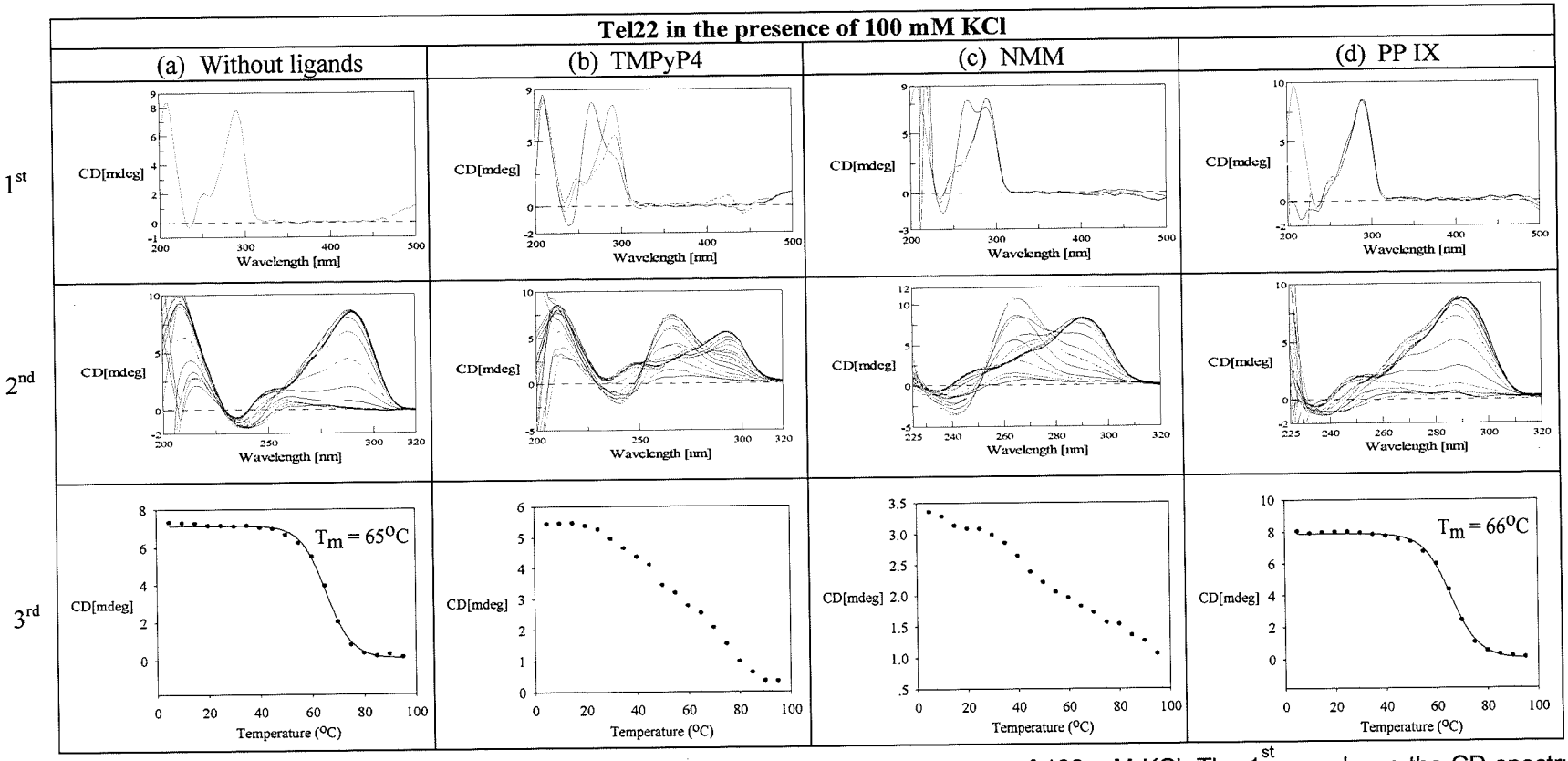

Figure 11 Effects of ligands on the G-quadruplex structure adopted by Tel22 in the presence of 100 mM KCl. The 1st row shows the CD spectrum of G-quadruplex without ligands (blue line) compared with those obtained in the presence of each ligand before and after T_m experiments (green and red lines, respectively). The 2nd row shows the CD spectra obtained at various temperatures (5-95°C) during T_m experiments. The last row shows the melting profiles in the absence or presence of each ligand (3 eq.) as indicated in the column heading.

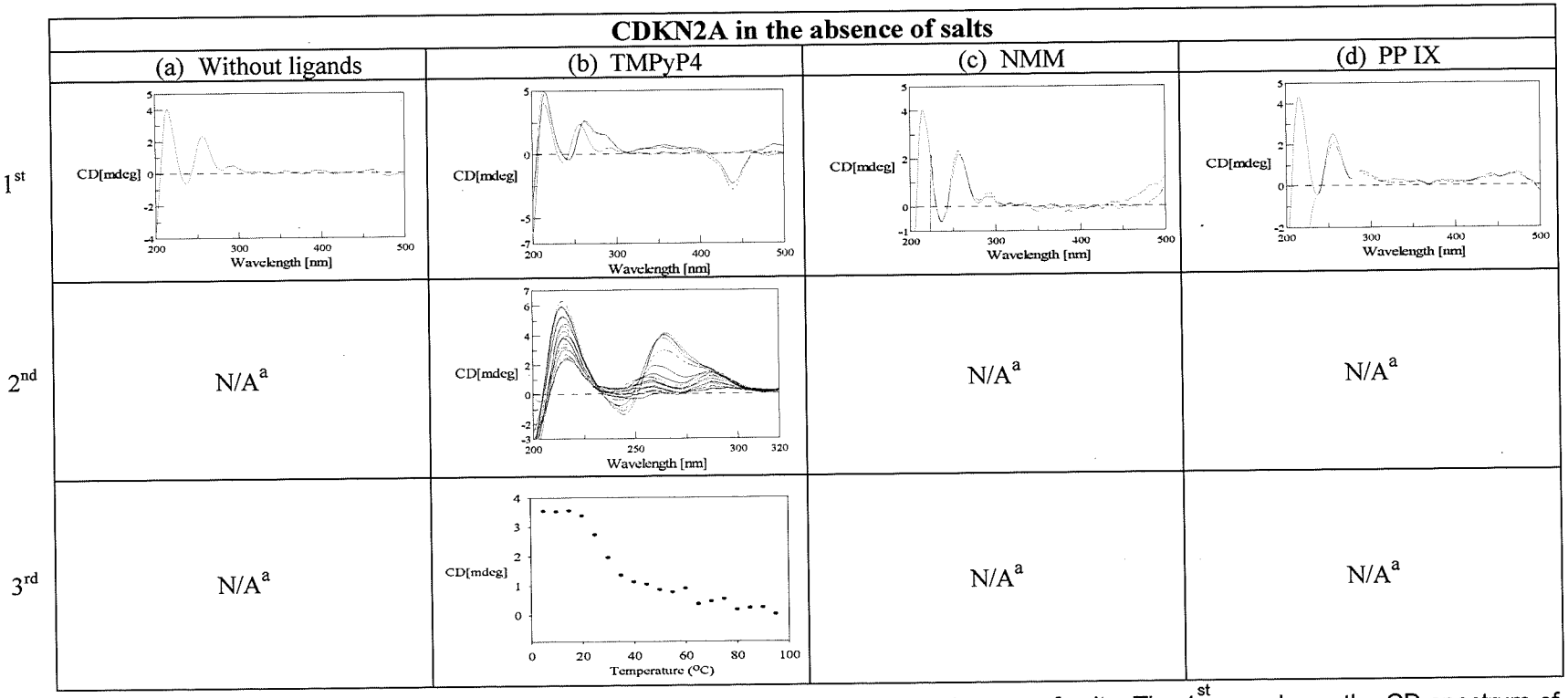

Figure 12 Effects of ligands on the G-quadruplex structure adopted by CDKN2A in the absence of salts. The 1st row shows the CD spectrum of G-quadruplex without ligands (blue line) compared with those obtained in the presence of each ligand before and after T_m experiments (green and red lines, respectively). The 2nd row shows the CD spectra obtained at various temperatures (5-95°C) during T_m experiments. The last row shows the melting profiles in the absence or presence of each ligand (3 eq.) as indicated in the column heading. [a]Melting experiments could be conducted only when G-quadruplex formation was induced by the ligand.

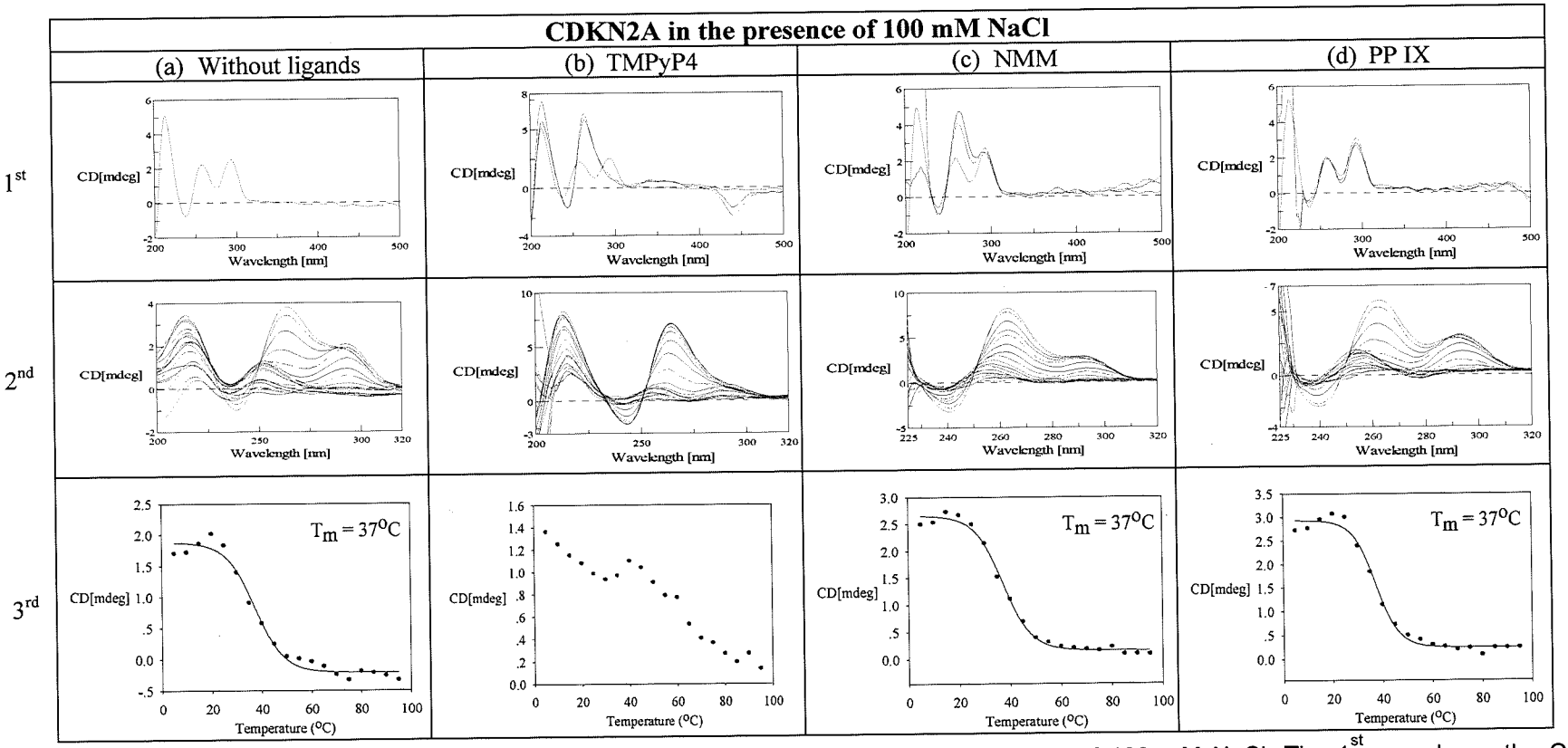

Figure 13 Effects of ligands on the G-quadruplex structure adopted by CDKN2A in the presence of 100 mM NaCl. The 1st row shows the CD spectrum of G-quadruplex without ligands (blue line) compared with those obtained in the presence of each ligand before and after T_m experiments (green and red lines, respectively). The 2nd row shows the CD spectra obtained at various temperatures (5-95°C) during T_m experiments. The last row shows the melting profiles in the absence or presence of each ligand (3 eq.) as indicated in the column heading.

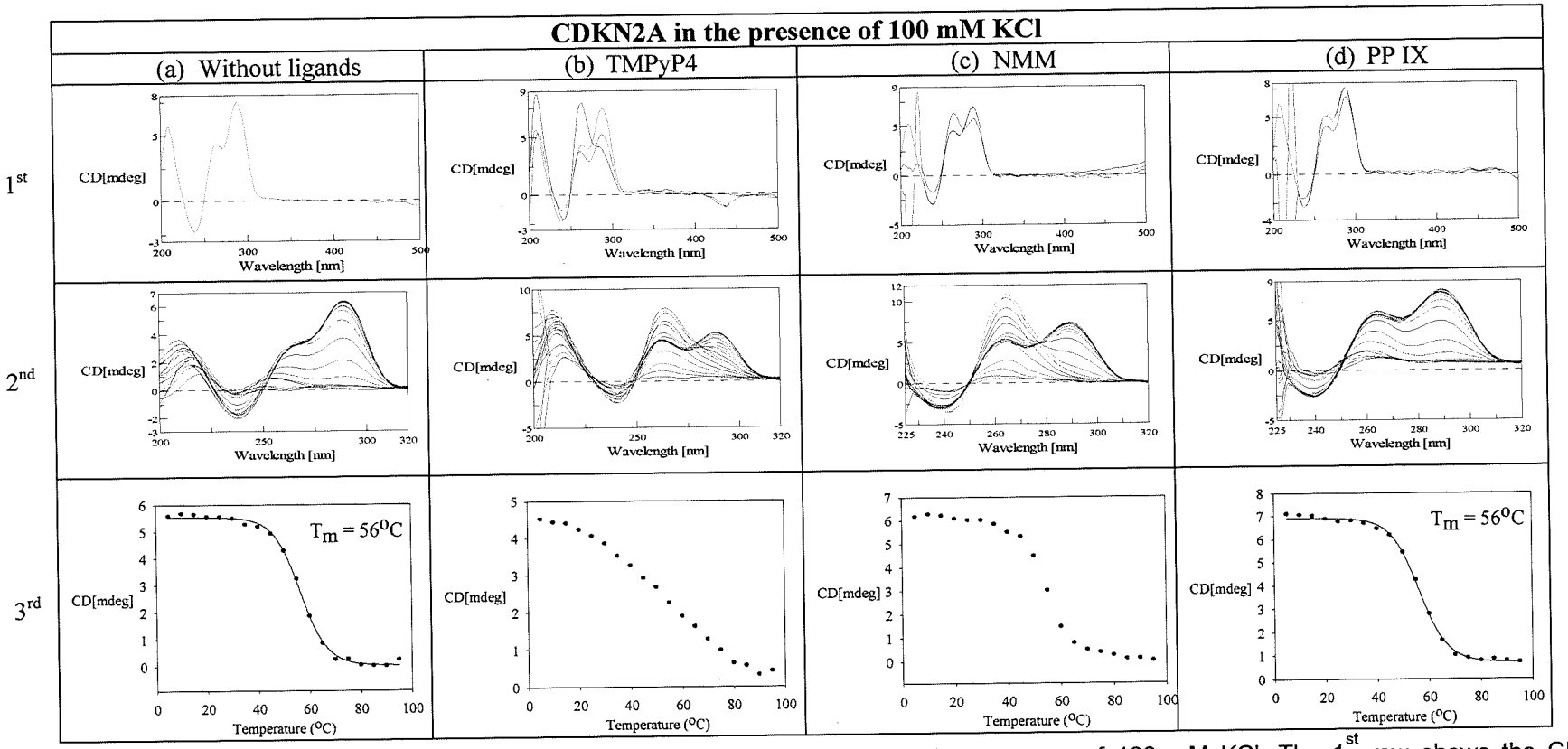

Figure 14 Effects of ligands on the G-quadruplex structure adopted by CDKN2A in the presence of 100 mM KCl. The 1st row shows the CD spectrum of G-quadruplex without ligands (blue line) compared with those obtained in the presence of each ligand before and after T_m experiments (green and red lines, respectively). The 2nd row shows the CD spectra obtained at various temperatures (5-95°C) during T_m experiments. The last row shows the melting profiles in the absence or presence of each ligand (3 eq.) as indicated in the column heading.

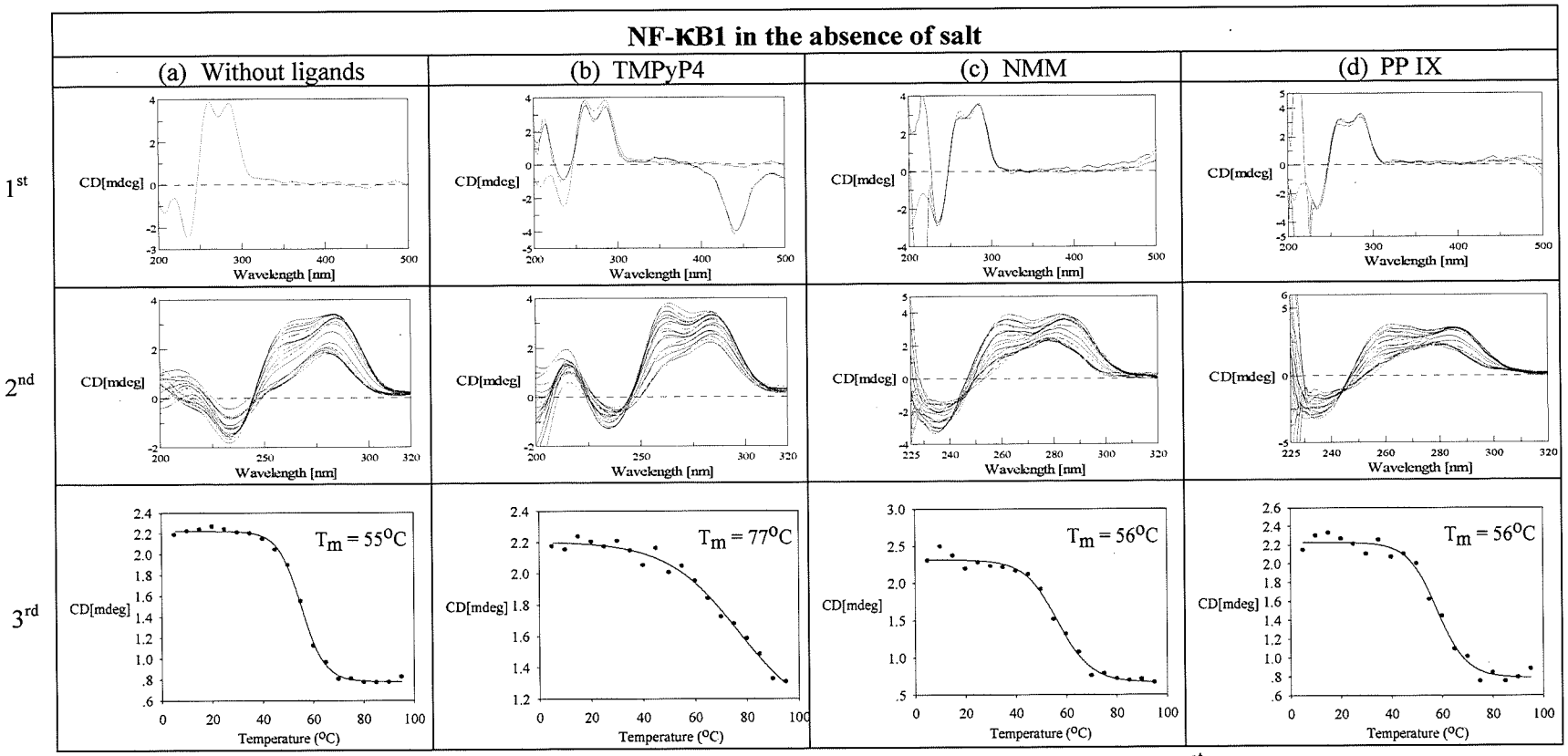

Figure 15 Effects of ligands on the G-quadruplex structure adopted by NF-κB1 in the absence of salt. The 1st row shows the CD spectrum of G-quadruplex without ligands (blue line) compared with those obtained in the presence of each ligand before and after T_m experiments (green and red lines, respectively). The 2nd row shows the CD spectra obtained at various temperatures (5-95°C) during T_m experiments. The last row shows the melting profiles in the absence or presence of each ligand (3 eq.) as indicated in the column heading.

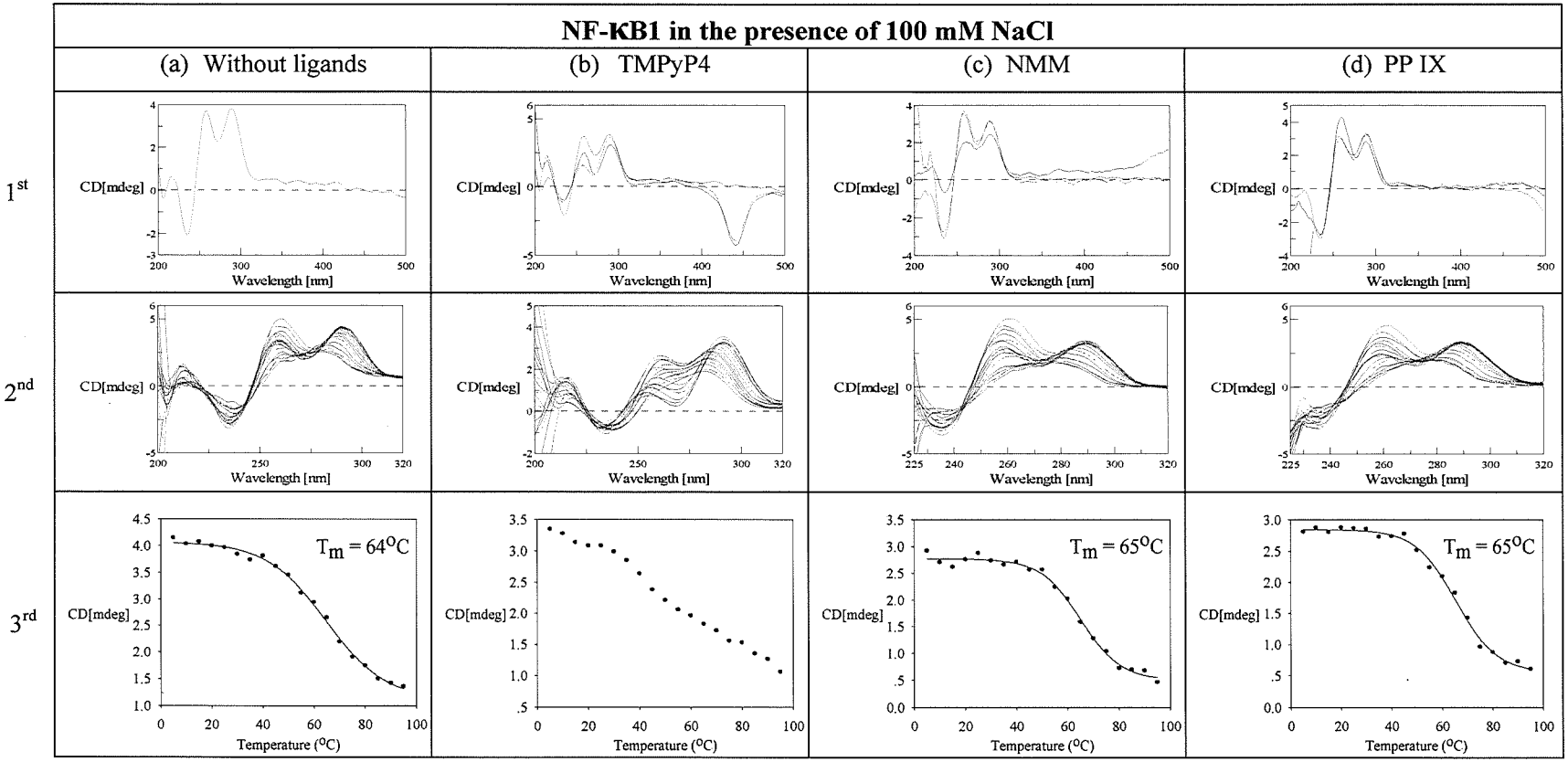

Figure 16 Effects of ligands on the G-quadruplex structure adopted by NF-κB1 in the presence of 100 mM NaCl. The 1st row shows the CD spectrum of G-quadruplex without ligands (blue line) compared with those obtained in the presence of each ligand before and after T_m experiments (green and red lines, respectively). The 2nd row shows the CD spectra obtained at various temperatures (5-95°C) during T_m experiments. The last row shows the melting profiles in the absence or presence of each ligand (3 eq.) as indicated in the column heading.

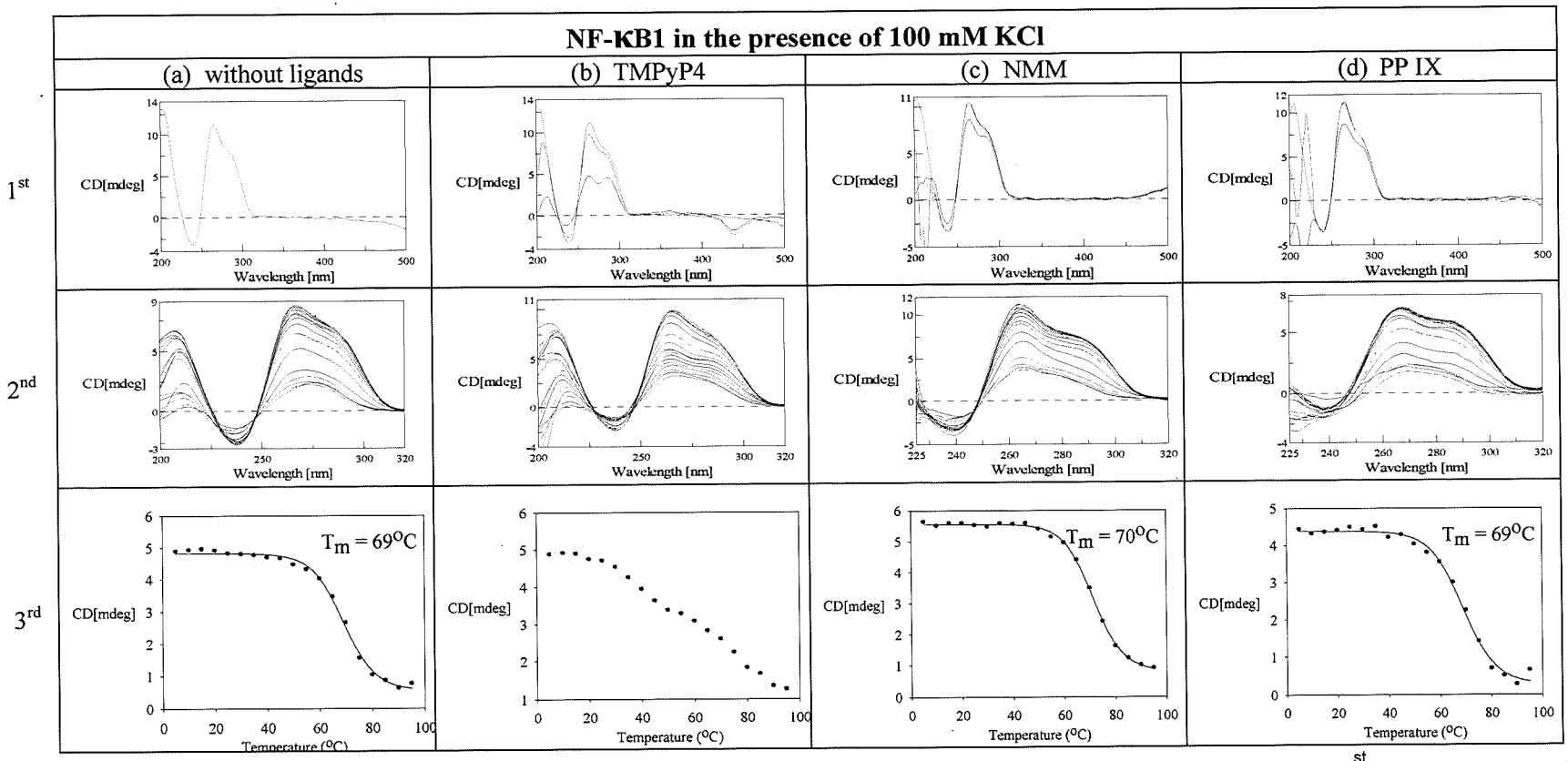

Figure 17 Effects of ligands on the G-quadruplex structure adopted by NF-κB1 in the presence of 100 mM KCl. The 1st row shows the CD spectrum of G-quadruplex without ligands (blue line) compared with those obtained in the presence of each ligand before and after T_m experiments (green and red lines, respectively). The 2nd row shows the CD spectra obtained at various temperatures (5-95°C) during T_m experiments. The last row shows the melting profiles in the absence or presence of each ligand (3 eq.) as indicated in the column heading.

In addition, NMM also had no influence on almost all of the formed G-quadruplex structures, except those adopted by Tel22 and CDKN2A in the presence of 100 mM KCl. Normally, NMM acts as a weak G-quadruplex binder because at pH 7.4, which was used in this experiment, a negative charge is generated at the terminal carboxylic group to prevent favorable electrostatic interactions with DNA. Furthermore, NMM has also been reported to specifically bind to parallel G-quadruplex structures.[35]

G-quadruplex induction by TMPyP4

CDKN2A could not adopt G-quadruplex structures in the absence of salts. Only TMPyP4 could induce G-quadruplex formation, as indicated by the change in the CD pattern after adding 3 eq. of the ligand. The positive peak near 255 nm indicative of unstructured DNA, was shifted to around 260 nm, while an additional positive peak near 290 nm was produced. These indicated the formation of a mixed parallel/antiparallel G-quadruplex structure. The change in the chirality of the proximal chemical environment of TMPyP4 gave an additional negative peak around 440 nm as a result of the interactions between the DNA and TMPyP4. Then, melting experiments were conducted. The CD spectra obtained showed that as temperature was increased from 5°C to 95°C, the intensity of the positive peak near 260 nm rapidly decreased to be comparable with that of the positive peak near 290 nm at around 35°C, indicating the presence of mixed parallel/antiparallel G-quadruplex structure, as evidenced by the two positive peaks near 260 and 290 nm with equal intensities. It is possible that there was a mixture of two major G-quadruplex structures with different melting temperatures, *i.e.*, 30°C and 65°C, which were obtained by monitoring the changes in the CD signals at 260 and 295 nm, representing parallel

and mixed parallel/antiparallel G-quadruplex structures, respectively (Figure 18). Therefore, TMPyP4 induced a mixture of structures comprising the less stable parallel G-quadruplex structure with a T_m of 30°C and the more stabilized mixed parallel/antiparallel G-quadruplex structure with a T_m of 65°C.

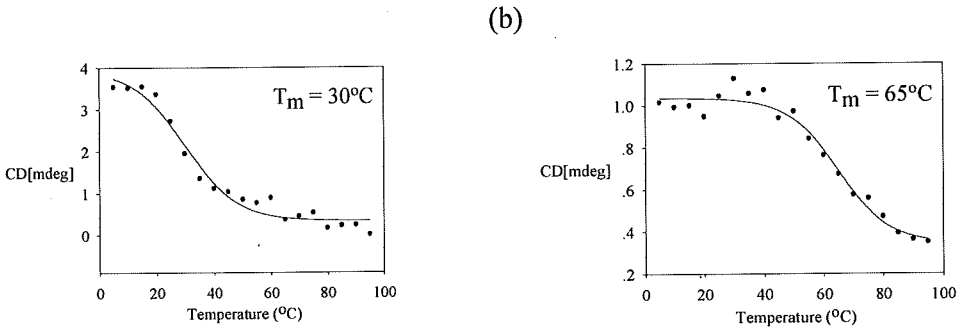

Figure 18 Melting profiles and melting temperatures of the G-quadruplex structure adopted by CDKN2A in the presence of 3 eq. of TMPyP4 when monitored at (a) 260 and (b) 295 nm, respectively.

Destabilizing effects of TMPyP4

In the presence of 100 mM NaCl, Tel22 apparently adopted an anti-parallel G-quadruplex structure, as indicated by a characteristic positive peak near 295 nm, a negative peak near 265 nm, and a smaller positive peak near 245 nm. The anti-parallel G-quadruplex structure demonstrated thermal stability with a melting temperature of 56°C. After adding of 3 eq. of TMPyP4, the CD pattern remained, except for the emergence of a negative characteristic peak of TMPyP4 binding near 440 nm. In addition, the melting profile showed a monophasic curve with a T_m of 50°C, which is 6°C smaller than that obtained without ligands. This suggested that TMPyP4 could bind to and destabilize the formed anti-parallel G-quadruplex structure. In addition, after adding 3 eq. of TMPyP4, the decrease in CD intensity without major changes in the CD pattern of Tel22 was found,

which might be caused by the loss of some G-quadruplex structures as a result of destabilization. Our results are consistent with the previous report by Gray et al.[36] Their results showed that upon adding 2 eq. of TMPyP4 to the anti-parallel G-quadruplex structure adopted by this telomeric sequence in the presence of 100 mM NaCl, the intensities of the two characteristic peaks around 260 and 295 nm decreased. The authors explained this phenomenon as a topological change towards the mixed parallel/antiparallel structure although the amount of the ligand added was insufficient to induce complete structural transition in this study.

Stabilizing effects of TMPyP4

NF-KB1 could adopt a mixed parallel/antiparallel G-quadruplex structure in the absence of salts. Upon adding 3 eq. of TMPyP4, the change in the CD patterns was not observed, except for an occurrence of a negative characteristic peak of TMPyP4 binding near 440 nm. However, the melting experiments demonstrated that the binding of TMPyP4 to the G-quadruplex structure significantly increased its thermal stability with a ΔT_m of 22°C. This indicated that TMPyP4 could stabilize the formed mixed parallel/antiparallel G-quadruplex structure without any topological changes.

Induction of topological changes by TMPyP4

Tel22 could form an anti-parallel G-quadruplex structure in the absence of salts with the T_m of 27°C. Upon the addition of 3 eq. of TMPyP4, the CD spectrum was immediately and dramatically changed such that the maximum near 250 nm emerged, and the maximum near 295 nm was shifted to 290 nm, whereas the minimum near 265 nm disappeared. These results indicated the presence of a mixed parallel/anti-parallel

G-quadruplex structure with higher thermal stability, as suggested by the 5°C increase in the T_m value. Therefore, TMPyP4 showed the ability to reform the preformed anti-parallel G-quadruplex structure to a more stable mixed parallel/antiparallel G-quadruplex structure.

In a similar manner, a mixed parallel/antiparallel G-quadruplex structure adopted by CDKN2A in the presence of 100 mM NaCl was immediately converted to a parallel G-quadruplex structure, as indicated by a more pronounced peak around 260 nm and reduced peak intensity around 290 nm. However, the CD spectra obtained during the melting experiments showed that not only a parallel G-quadruplex was generated, but also another mixed parallel/antiparallel G-quadruplex structure also emerged, as supported by the rapidly decreased intensity of the positive peak around 260 nm compared to that of the positive peak around 290 nm when temperature was increased from 5°C to 95°C. The emergence of this mixed parallel/antiparallel G-quadruplex structure was obviously observed at 45°C, as indicated by the presence of two positive peaks near 260 and 290 nm with similar intensities. These results can reflect the presence of structures with different stabilities. When the changes in the CD signals were monitored at 260 and 295 nm, the T_m values of 38 and 63°C were obtained, respectively. Therefore, it is possible that TMPyP4 could induce a mixture of structures, containing a moderately stable parallel G-quadruplex structure with a T_m of 38°C and a stable mixed parallel/antiparallel G-quadruplex structure with a T_m of 63°C.

(a) (b)

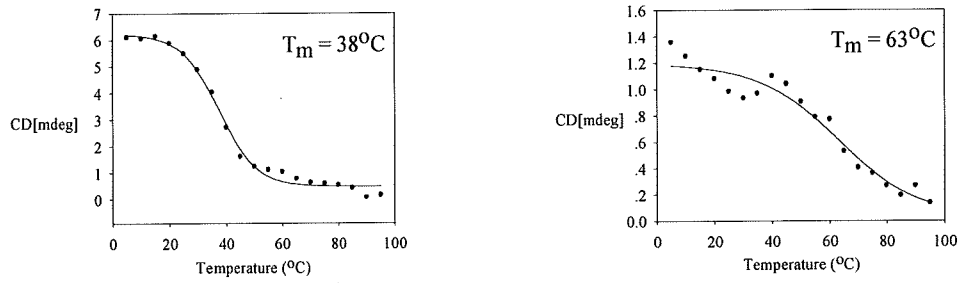

Figure 19 Melting profiles and melting temperatures of the G-quadruplex structure adopted by CDKN2A in the presence of 100 mM NaCl upon adding 3 eq. of TMPyP4, when monitored at (a) 260 and (b) 295 nm, respectively.

Similarly, the mixed parallel/antiparallel G-quadruplex structure adopted by NF-κB1 in the presence of 100 mM NaCl also underwent topological changes induced by TMPyP4, as indicated by the decreased intensity of the positive peak near 260 nm. An overlay of nineteen spectra obtained during the melting experiments revealed coexistence of two different mixed parallel/antiparallel G-quadruplex structures, as suggested by the decreased intensity and slight red shift of the positive peak around 290 nm, as well as the more pronounced intensity and slight blue shift of the positive peak around 260 nm with increasing temperature. However, we did not observe the expected biphasic melting profile at 295 nm with two distinct T_m values for coexisting mixed parallel/antiparallel G-quadruplex structures, which could be due to the insignificant difference of their stabilities.

Structural changes induced by various ligands have been previously observed and recently reviewed by Haider et al.[37] They remarked that the reason for structural changes after adding sufficient ligands could be to provide extended binding platforms for ligands to associate by either extending G-quartet surfaces or forming additional planar

dinucleotide pairings. Our results showed that after adding TMPyP4, G-quadruplex topologies were changed to either parallel or mixed parallel/antiparallel G-quadruplex structures. It is possible that parallel G-quadruplex structures containing three propeller loops yield maximum available quartet surface area for ligand interactions at both 3' and 5' termini (Figure 20a), while mixed parallel/antiparallel G-quadruplex structures can provide an available surface area at only one end (Figure 20b). In the case of anti-parallel topology, the surface areas are shielded from ligand interactions by either the lateral or diagonal loops present in their topologies (Figure 20c).

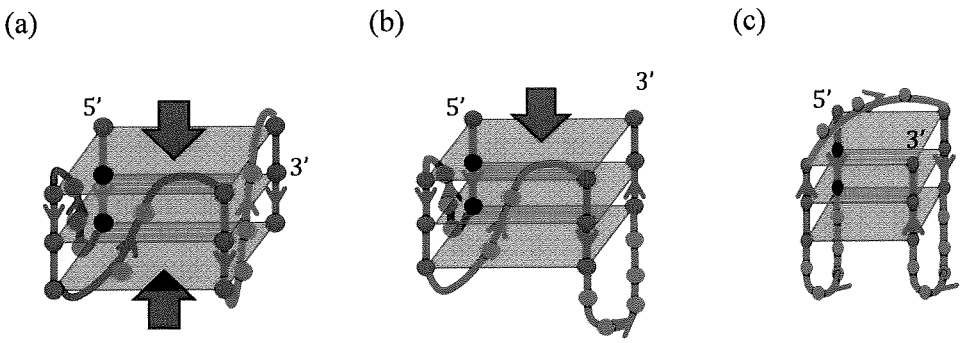

Figure 20 Illustrations showing the topologies of (a) parallel, (b) mixed parallel/antiparallel, and (c) anti-parallel G-quadruplex structures, along with the plausible surface areas available for ligand interactions indicated by red arrows.

Topological changes by TMPyP4 after annealing

Another effect of TMPyP4 on G-quadruplex structures observed in this study was the topological change of G-quadruplex structures that occurred after heating. Three common features of this effect are i. no dramatic change in the CD spectrum was observed after adding 3 eq. of ligands, ii. more pronounced positive peak around 260 nm would be observed as the temperature was increased during melting experiments, suggesting the

presence of a conformation with substantial parallel component, and iii. the topology of G-quadruplex structures was changed after melting experiments. For better understanding, the results obtained for this effect are summarized in Figure 21. In addition, plots of the ellipticity at 260 nm as a function of temperature were constructed to monitor the formation of parallel G-quadruplex structures.

As shown in Figure 21, TMPyP4 displayed such effect on the G-quadruplex structures adopted by Tel22, CDKN2A, and NF-κB1 only in the presence of 100 mM KCl. In the case of Tel22 and CDKN2A, the mixed parallel/antiparallel G-quadruplex structures adopted in the presence of 100 mM KCl were not substantially changed after adding 3 eq. of TMPyP4, as indicated by no dramatic change in the CD spectra (1^{st} row, columns a and b in Figure 21). The CD spectra obtained during melting experiments (2^{nd} row, columns a and b in Figure 21) revealed that as the temperature was increased, a positive peak around 295 nm was reduced, and a prominent positive peak around 260 nm was observed. Thus, changes in the ellipticity at 260 nm were monitored as a function of temperature (3^{rd} row, columns a and b in Figure 21). These results showed that a more pronounced positive peak around 260 nm was generated at ~40°C and reached the maximum ellipticity at ~60°C, indicating the formation of a G-quadruplex structure with substantial parallel component as the temperature was increased. Afterwards, as the samples were heated further, this positive peak around 260 nm continuously decreased, implying the melting process of the recently formed G-quadruplex structure. Based on these results, the interaction of TMPyP4 on G-quadruplex structures is proposed that both TMPyP4 and heat could collaboratively induce a structural transition to parallel G-quadruplex structure. To prove this model, the G-quadruplex structures adopted by

either Tel22 or CDKN2A in the presence of 100 mM KCl and 3 eq. of TMPyP4 were prepared, then heated at 95°C for 5 min, and slowly cooled down to room temperature. In the case of Tel22, the CD spectrum (1st row, column a in Figure 22) displayed a similar pattern to that previously obtained after melting experiments (Figure 21, 1st row, column a, red line), which confirmed that the addition of 3 eq. of TMPyP4 along with heating caused topological changes of G-quadruplex structures. However, as shown in Fig. 22 (1st row, column a), the new topology formed was not the expected parallel G-quadruplex structure, as indicated by the presence of a positive peak around 295 nm. Hence, to provide more information, the sample was subject to melting experiments, and the results are shown in Figure 22 (2nd to 4th rows, column a). Two melting curves, monitored at either 260 or 295 nm, were constructed to determine the melting temperatures of parallel and mixed parallel/antiparallel G-quadruplex structures, respectively. The resulting melting temperatures revealed that the sample might contain a mixture of two distinct G-quadruplex structures with different thermal stabilities, including a thermally stable parallel G-quadruplex structure with a T_m of 80°C and a mixed parallel/antiparallel G-quadruplex structure with a T_m of 66°C. Interestingly, the T_m value of the latter is similar to that of a mixed parallel/antiparallel G-quadruplex structure adopted by Tel22 in the presence of 100 mM KCl without ligands. Therefore, the mixture might contain a newly adopted parallel G-quadruplex structure as a result of the interaction with TMPyP4 in the presence of heat, as well as a non-interacting mixed parallel/antiparallel G-quadruplex structure. Moreover, the same results were also observed in case of CDKN2A, as shown in Figure 22 (column b).

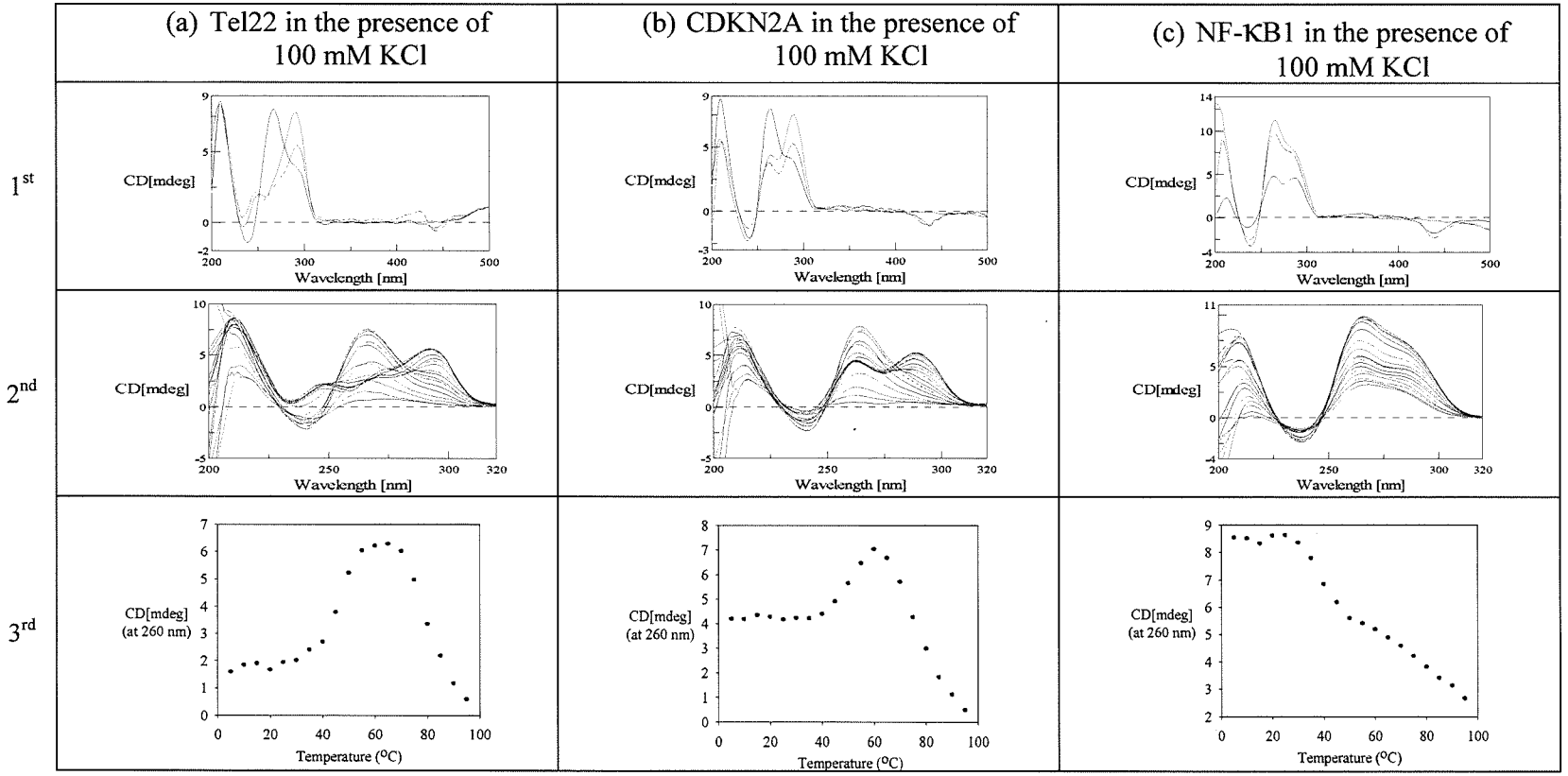

Figure 21 Effects of TMPyP4 on the G-quadruplex structures adopted by (a) Tel22, (b) CDKN2A and (c) NF-κB1 in the presence of 100 mM KCl. The 1st row shows the CD spectra of G-quadruplex without the ligand (blue line) compared with those obtained in the presence of ligand before and after T_m experiments (green and red lines, respectively). The 2nd row shows the CD spectra obtained at various temperatures (5-95°C) during T_m experiments. The last row shows the plots of ellipticity at 260 nm as a function of temperature.

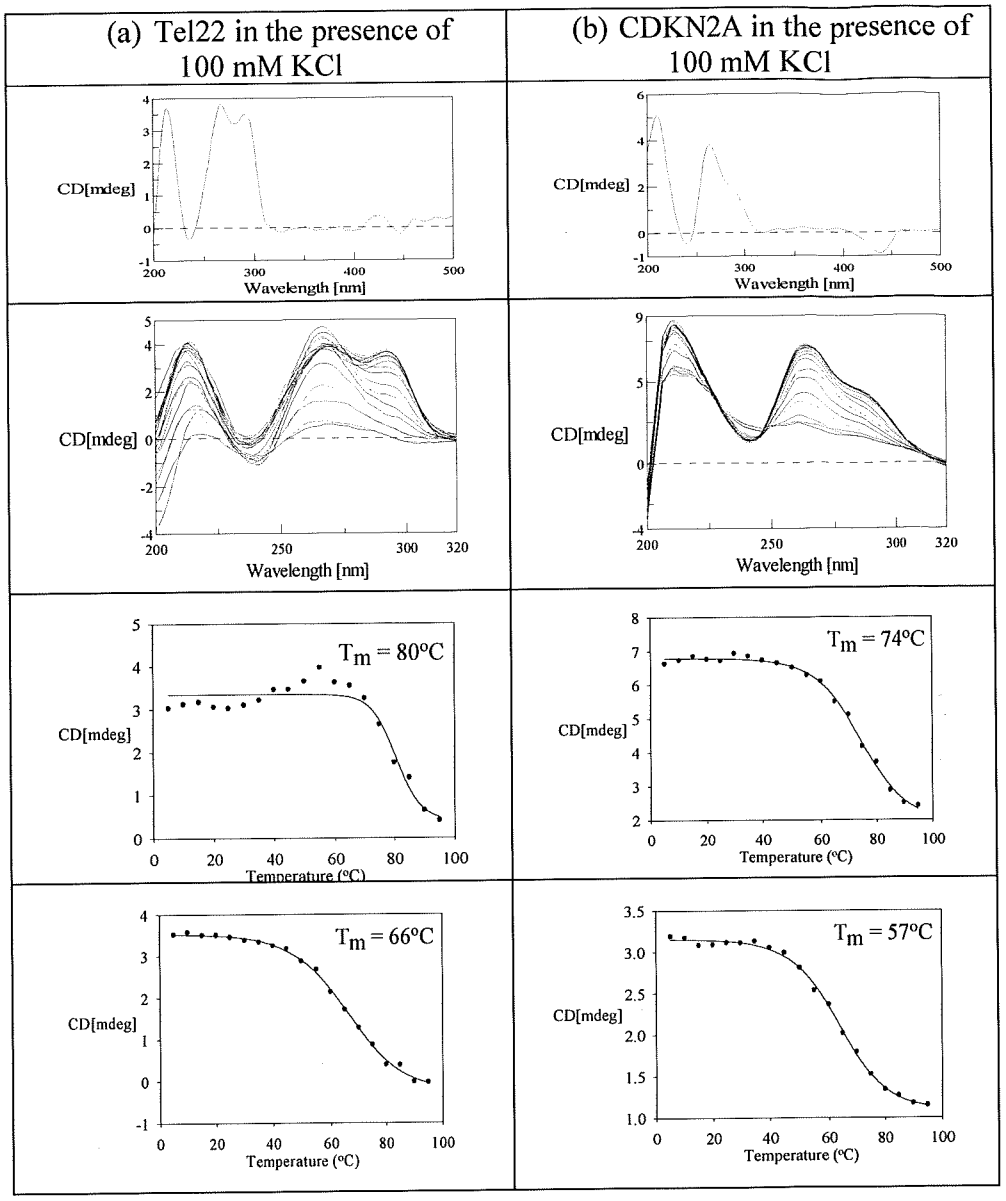

Figure 22 The results obtained from annealing experiments of G-quadruplex structures adopted by (a) Tel22 and (b) CDKN2A in the presence of 100 mM KCl and TMPyP4. The 1st row shows the CD spectra of G-quadruplex obtained after annealing with the ligand. The 2nd row shows the CD spectra obtained at various temperatures (5-95°C) during T_m experiments. The 3rd and 4th rows show the melting profiles monitored at 260 and 295 nm, respectively.

Interestingly, the results were quite different for the G-quadruplex topology of NF-κB1 in the presence of 100 mM KCl and 3 eq. of TMPyP4. As shown in Figure 21, although annealing also caused some changes in the G-quadruplex topology of NF-κB1, the CD patterns obtained during the melting experiments were distinct from the other two cases. In fact, the positive peak around 260 nm actually decreased with temperature during the melting experiments with a biphasic character, as shown in Figure 21 (3^{rd} row, column c). It is possible that the addition of 3 eq. of TMPyP4 induced coexistence of two different mixed parallel/antiparallel G-quadruplex structures with different thermal stabilities. However, the change in the CD pattern after the melting experiments (Figure 21, 1^{st} row, column c, red line), indicated the formation of another mixed parallel/antiparallel G-quadruplex structure adopted during melting experiments. To prove this assumption, NF-κB1 in the presence of 100 mM KCl and 3 eq. of TMPyP4 underwent an annealing experiment by heating at 95°C for 5 min, and was allowed to cool down to room temperature. A similar CD pattern (Figure 23a) was observed as compared to that obtained after the previous melting experiment (Figure 21, 1^{st} row, column c, red line). According to in occurrence of the prominent peak around 260 nm during melting experiment, the melting temperature was determined at 295 nm instead. From the resulting monophasic melting curve (Figure 23c), the T_m value was 61°C, which is 8°C smaller than that obtained without ligands. These results suggested that TMPyP4 might have destabilizing effects on NF-κB1 by changing its topology to a less stable G-quadruplex structure.

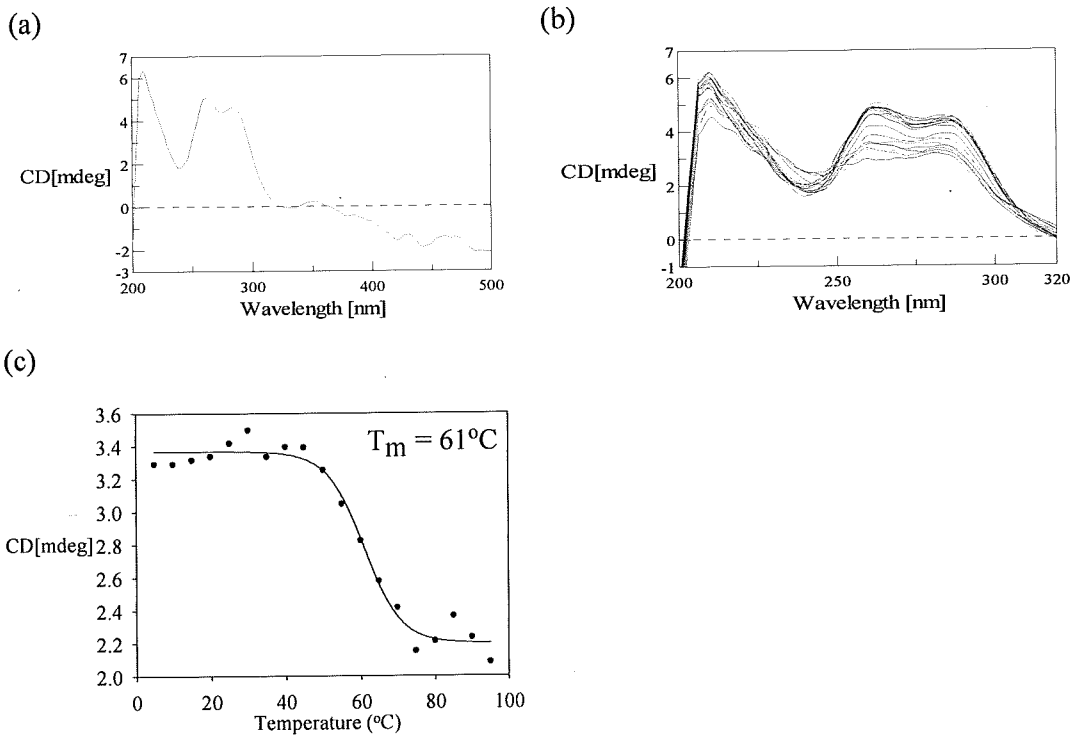

Figure 23 Results obtained from annealing experiments of G-quadruplex structures adopted by NF-KB1 in the presence of 100 mM KCl and TMPyP4, (a) the CD spectra of G-quadruplex obtained after annealing with the ligand, (b) the CD spectra obtained at various temperatures (5-95°C) during T_m experiments, and (c) the melting profile monitored at 295 nm.

Topological changes by NMM after annealing

A weak G-quadruplex binding ligand, NMM, could not display any effects on the G-quadruplex structures of our interests, except those adopted by Tel22 and CDKN2A in the presence of 100 mM KCl. In addition, the effects of NMM were consistent with those of TMPyP4, causing topological changes of these G-quadruplex structures after annealing process. The obtained results along with the melting plots monitored at 260 nm are summarized in Figure 24.

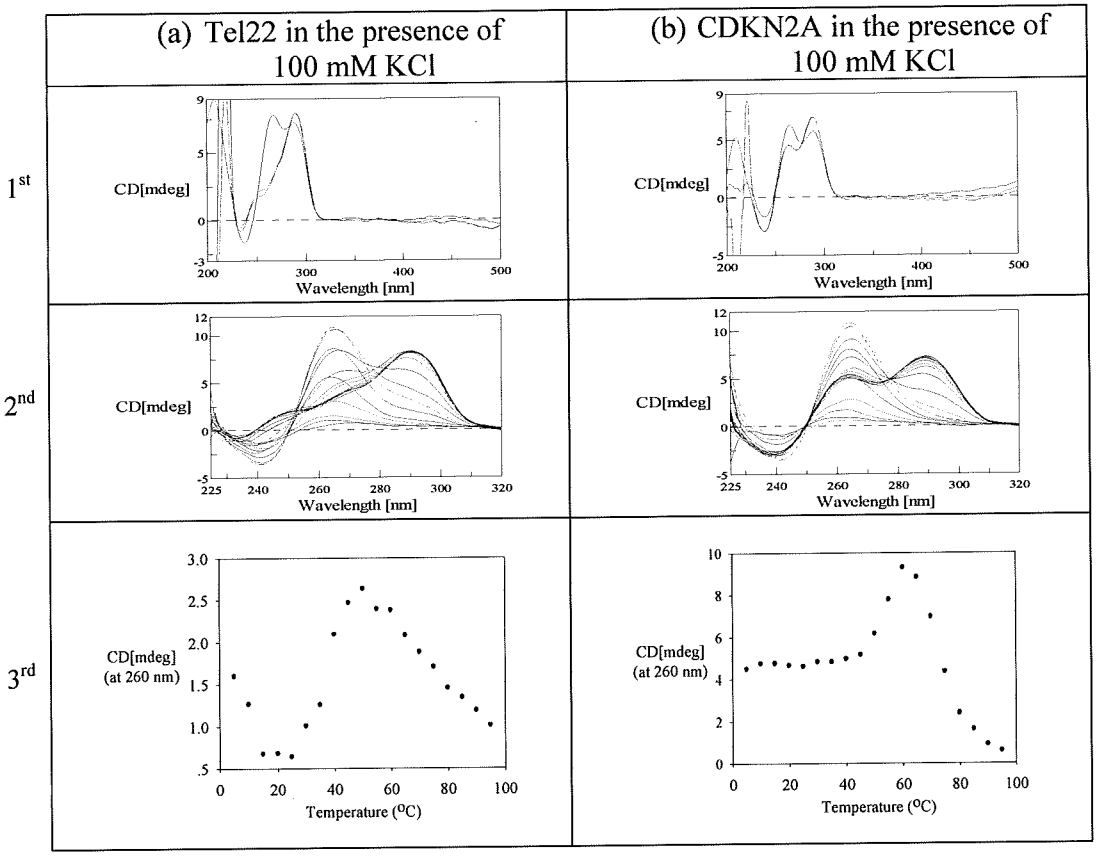

Figure 24 Effects of NMM on the G-quadruplex structures adopted by (a) Tel22, (b) CDKN2A and (c) NF-κB1 in the presence of 100 mM KCl. The 1st row shows the CD spectra of G-quadruplex without ligand (blue line) compared with those obtained in the presence of each ligand before and after T_m experiments (green and red lines, respectively). The 2nd row shows the CD spectra obtained at various temperatures (5-95°C) during T_m experiments. The last row shows the plots of ellipticity at 260 nm as a function of temperature.

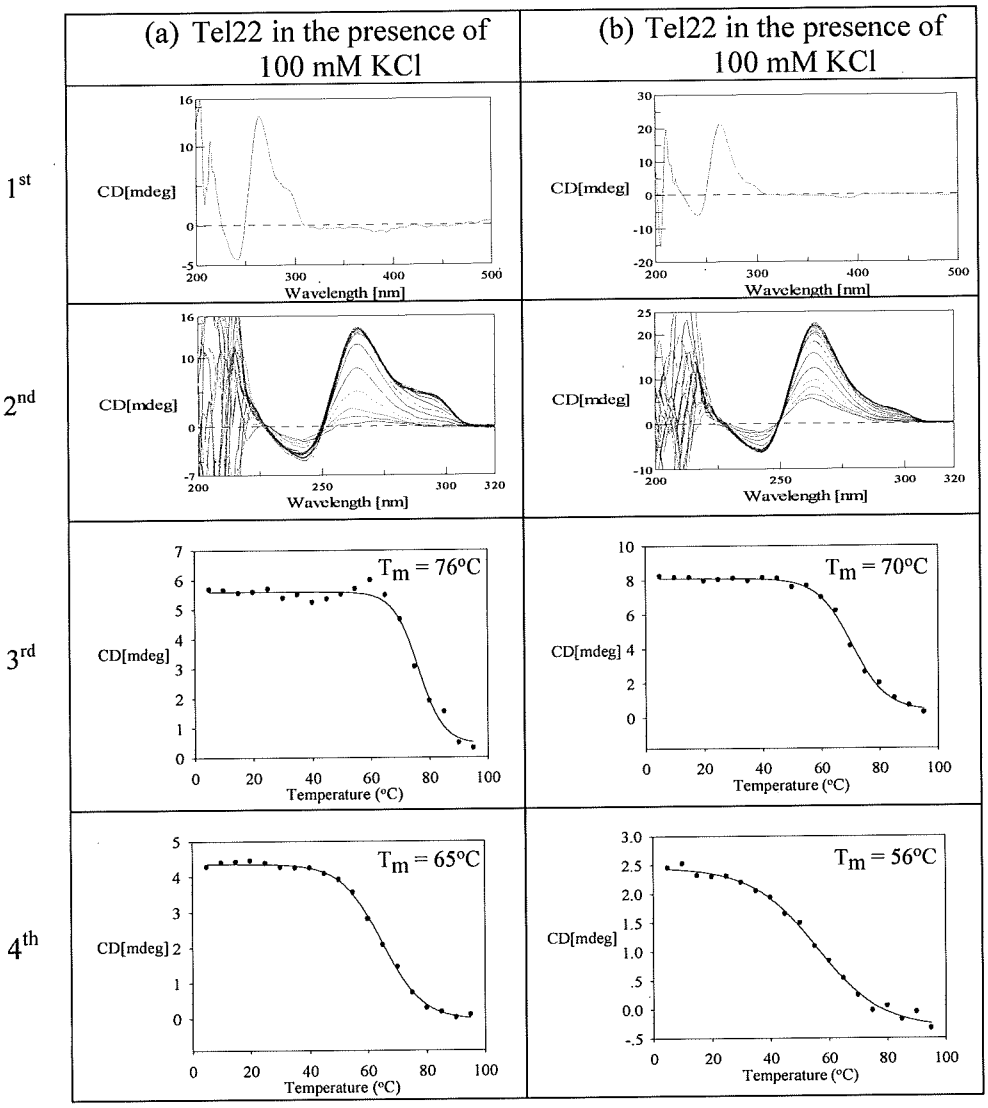

Figure 25 Results obtained from annealing experiments of G-quadruplex structures adopted by (a) Tel22 and (b) CDKN2A in the presence of 100 mM KCl and NMM. The 1st row shows the CD spectra of G-quadruplex obtained after annealing with ligand. The 2nd row shows the CD spectra obtained at various temperatures (5-95°C) during T_m experiments. The 3rd and 4th rows show the melting profiles monitored at 260 and 295 nm, respectively.

In addition, the G-quadruplex structures adopted by either Tel22 or CDKN2A in the presence of 100 mM KCl and 3 eq. of NMM were also prepared, then heated at 95°C for 5 min, and slowly cooled down to room temperature. The results shown in Figure 25 were also consistent with those obtained using TMPyP4, indicating that not only TMPyP4, but also NMM, could cause topological changes of G-quadruplex structures when annealed by heating.

When the G-quadruplex structures adopted by Tel22 and CDKN2A in the presence of 100 mM KCl were exposed to either TMPyP4 or NMM, a structural change to parallel G-quadruplex structures was observed, possibly for providing maximum surface area for ligand interactions. However, in these cases, heating was also required in addition to presence of ligands. It is possible that those G-quadruplex structures were stabilized by potassium with high stabilizing power,[30] and thus, they were too thermally stable to rearrange to adopt a suitable topology for ligand binding without heating. The additional heating step might help loosen the stable G-quadruplex structure, allowing topology rearrangement to be parallel structures upon the interactions with ligands. For better understanding, a proposed mechanism is shown in Figure 26.

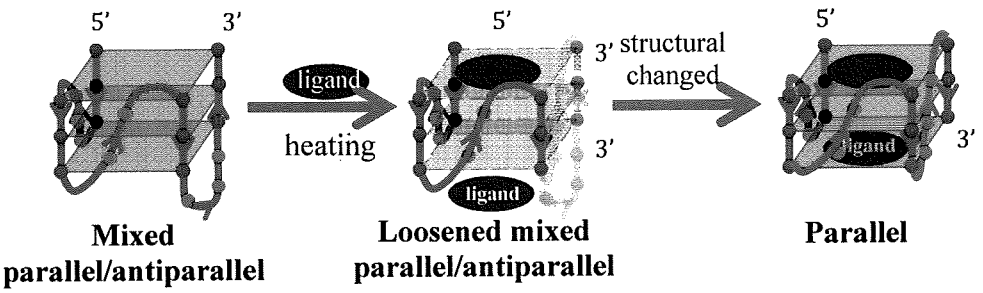

Figure 26 Proposed mechanism for structural rearrangement of G-quadruplex structures caused by ligands, incorporated with heating.

Although both the more potent TMPyP4 and the less potent NMM could cause structural changes of G-quadruplex structures, the latter required the presence of potassium ions. This phenomenon is consistent with a previous report by Nicoludis et al.,[35] who suggested that NMM could induce structural changes of the G-quadruplex structures adopted by telomeric sequence to a parallel topology. In addition, it was mentioned that this effect of NMM is potassium dependent although the mechanism of how NMM-induced structural rearrangement is specific to the presence of potassium ions remains questionable.[35]

Binding stoichiometries and binding constants of TMPyP4 to the G-quadruplex structures by UV absorption titration experiments

Among the three studied ligands, TMPyP4 could display the most prominent effect on the G-quadruplex structures formed by Tel22, CDKN2A, and NF-KB1. Thus, the binding interactions between TMPyP4 and the formed G-quadruplex structures were examined using UV-Visible absorption titration.

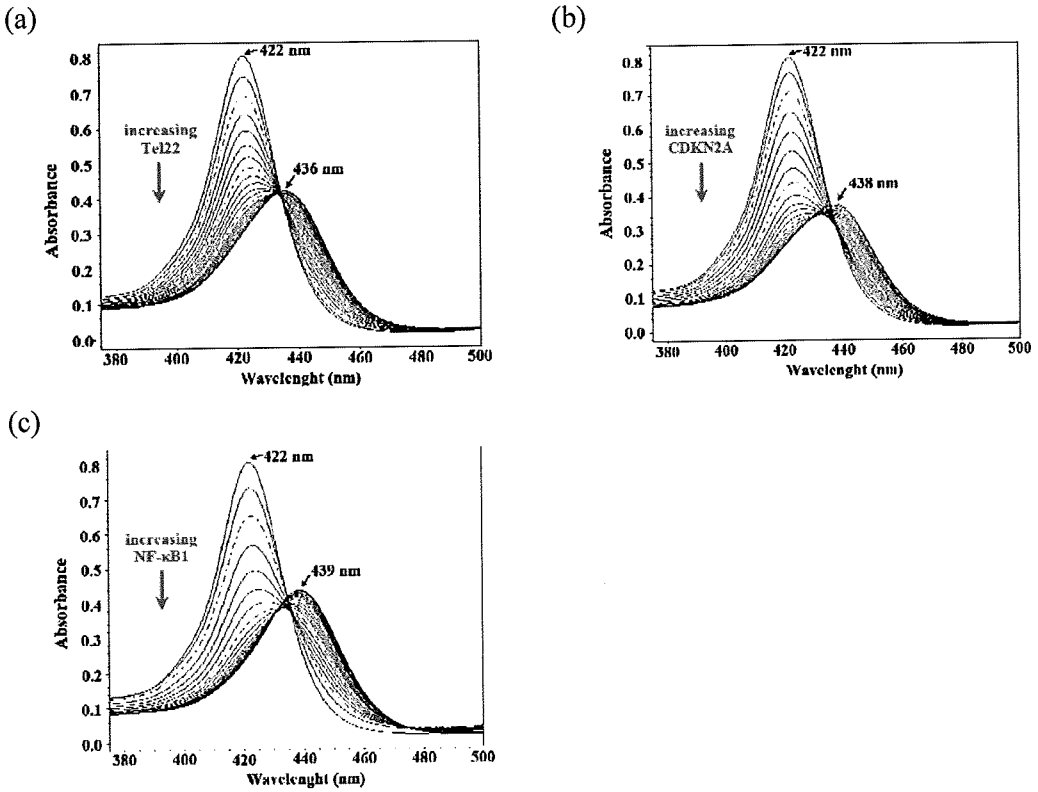

Figure 27 UV-Vis absorption titration spectra of TMPyP4 (approximately 3.5 μM) with (a) Tel22, (b) CDKN2A, and (c) NF-ΚB1 oligonucleotides in 1XTE (pH 7.4) in the presence of 100 mM KCl.

As shown in Figure 9, free TMPyP4 exhibited the Soret band at 422 nm. Following the additions of the G-quadruplex structures, red shifts and successive decreases in the intensity of the Soret band of free TMPyP4 were observed, the latter of which suggested its decreased concentrations. In addition, to determine the numbers of equivalent binding sites and the binding affinities of TMPyP4 for those sites, Scatchard analysis was applied. All Scatchard plots obtained are nonlinear, which may be caused by more than one binding sites for TMPyP4 in the G-quadruplex structures with unequal association constants.[38] Therefore, the Scatchard analysis with an assumption that there are two independent binding sites for TMPyP4 in the G-quadruplex structures was performed.

Subsequently, the plots between r and C_f were constructed (Figure 28), yielding hyperbola curves that could be fitted to obtain the binding parameters (n_1, n_2, K_1, K_2) by nonlinear regression. The binding stoichiometries (n_1, n_2) and binding constants (K_1, K_2) of TMPyP4 to three different G-quadruplex structures are reported in Table 4.

Table 3 UV absorption titration parameters for TMPyP4 upon titrations with the G-quadruplex structures formed in the presence of 100 mM KCl.

G-quadruplex structure	[TMPyP4][a] (μM)	[G-quadruplex][b] (μM)	Soret band shift (nm)	%Hypochromicity[c]
Tel22	3.54	2.35	14	61.07
CDKN2A	3.58	2.03	16	64.65
NF-ΚB1	3.57	2.12	17	66.80

[a] Initial concentrations of the free TMPyP4 at the beginning of titrations.

[b] Final concentration of G-quadruplexes at the end of titrations.

[c] ε_b = 88104, 79885, and 75105 M^{-1} cm^{-1} for Tel22, CDKN2A, and NF-ΚB1, respectively.

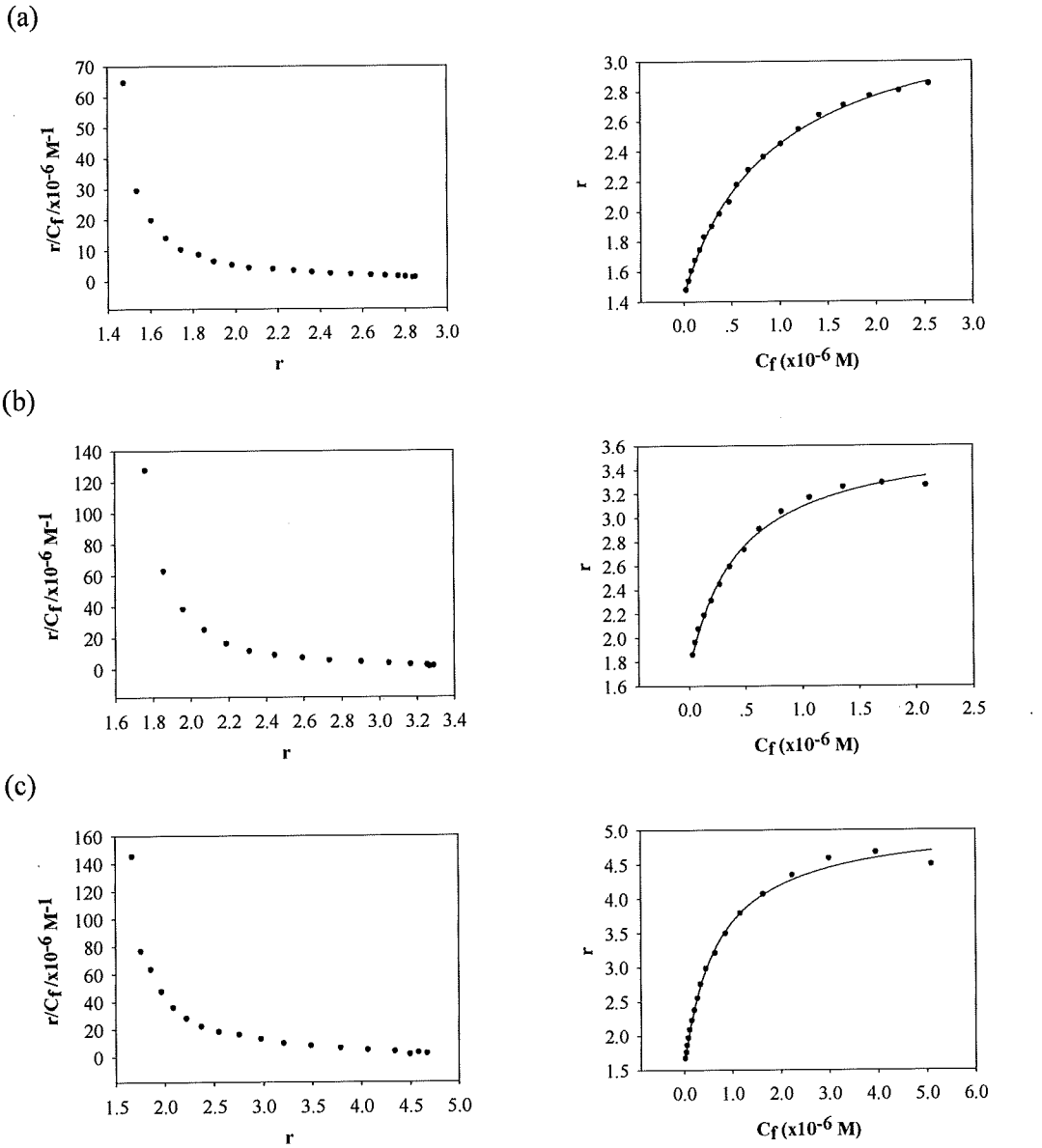

Figure 28 Scatchard plots (r/C_f versus C_f) (left) and plots of r versus C_f (right) for TMPyP4 with (a) Tel22, (b) CDKN2A, and (c) NF-KB1 G-quadruplexes.

Table 4 The binding stoichiometries (n_1, n_2) and binding constants (K_1, K_2) of TMPyP4 with the G-quadruplexes formed in the presence of 100 mM KCl.

G-quadruplexes	n_1	K_1 (M^{-1})	n_2	K_2 (M^{-1})
Tel22	1.45	3.00×10^9	1.95	1.04×10^6
CDKN2A	1.76	2.50×10^9	1.94	2.16×10^6
NF-KB1	1.57	1.14×10^{10}	3.56	2.81×10^6

In the presence of 100 mM KCl, Tel22 which is an extensively studied G-rich oligonucleotide derived from telomeric sequence could adopt a mixed parallel/antiparallel G-quadruplex structure, as indicated by circular dichroism results and also consistent with many previous reports.[39,40,41] The UV-Vis absorption titration results between TMPyP4 and this hybrid G-quadruplex showed 14 nm red shift and 61% hypochromicity. Two different binding sites with the higher and lower affinities were evaluated by the Scatchard analysis to give the *n* values of 1.45 (n_1) and 1.95 (n_2) with association constants of 3.00×10^9 M^{-1} (K_1) and 1.04×10^6 M^{-1} (K_2), respectively.

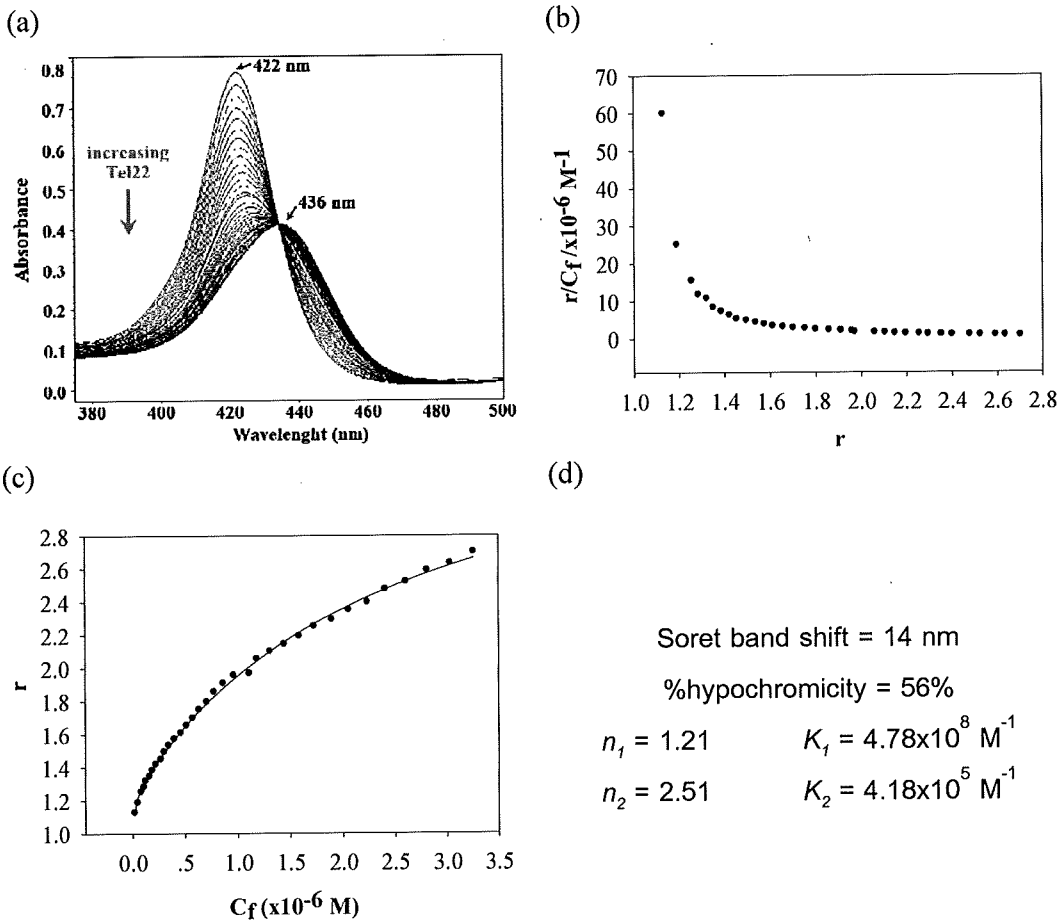

Figure 29 UV-Vis absorption titration results of TMPyP4 with Tel22 in the presence of 150 mM KCl (a) UV-Vis absorption titration spectra, (b) Scatchard plot (r/C_f versus C_f), (c) plot of r versus C_f, and (d) UV-vis absorption parameters.

Based on our results at two different concentrations of KCl, the overall binding stoichiometries were comparable, whereas both binding constants in the case of 100 mM KCl were clearly higher. These observations were consistent with the report by Zhang et al., who suggested that the increase in potassium concentration could reduce the binding affinity of TMPyP4 to G-quadruplex structure.[42]

The G-quadruplex structures adopted by CDKN2A and NF-KB1 produced larger red shifts and greater degrees of hypochromicities associated with the Soret band of TMPyP4 (422 nm) as compared with the values for Tel 22, which may result from different binding modes of TMPyP4 to these two G-quadruplex structures. The red shifts of 16 and 17 nm, accompanied by the %hypochromicity of 65% and 67% were produced by CDKN2A and NF-KB1 G-quadruplex structures, respectively. As described above, an intercalative binding mode exhibits at least 15 nm in red shift and at least 35% in %hypochromicity.[43] However, according to the report by Neidle et al., intercalation is clearly not the binding mode of TMPyP4 with G-quadruplex structures, as indicated by crystallographic studies.[44] In contrast, end-stacking of TMPyP4 on top of G-tetrads has been proposed by Phan et al. based on NMR studies.[45] In addition, external binding of TMPyP4 onto bases of the loops has been observed in the crystal structure of TMPyP4-quadruplex complex, as reported by Neidle et al.[44] Wei et al. have suggested the same two plausible binding modes of TMPyP4 to G-quadruplex structures with higher and lower binding affinities for end stacking and external binding modes, respectively.[42]

As a result, we proposed two plausible modes of TMPyP4 to in two G-quadruplex structures of our interest, including end stacking and external binding. The Scatchard showed two types of nonequivalent and independent binding sites with the higher and lower affinities, as indicated by the stronger (K_1) and weaker (K_2) binding constants, representing end-stacking and external binding modes, respectively. Although the binding parameters obtained in the cases of Tel22 and CDKN2A appeared comparable, they were quite different from the values for NF-KB1. These observations may arise from the different numbers of nucleotides in the loop regions. As mentioned earlier, NF-KB1 has a

propensity to form a three-tetrad G-quadruplex structure containing long three loops (range from 3 to 9 nucleotides), whereas the G-quadruplex structure adopted by CDKN2A contains 5, 2, and 3 nucleotide loops. The higher stoichiometry for external binding (n_2) obtained for NF-KB1 may result from the longer loops present in the formed G-quadruplex structure.

Effect of pH and potassium salt on a potential competition between duplex- and G-quadruplex or i-motif formation

In this study, the competition between duplex- and either G-quadruplex or i-motif formations within the promoter region of CDKN2A was investigated by applying various conditions, such as addition of KCl and/or decreasing the pH, to stimulate structural conversion of duplex to other structures, which was then monitored by CD spectroscopy, as shown in Figure 30.

At pH 7.4 and in the absence of salts, the two complementary strands of CDKN2A could form a B-form duplex, as indicated by the CD spectrum (Figure 30a) with two characteristic peaks, including a positive long wavelength band around 260-280 nm and a negative band around 245 nm.[46] Individual G-rich and C-rich strands could not adopt any structures under this condition (Figure 30a).

In the presence of 100 mM KCl, the G-rich strand of CDKN2A could adopt a mixed parallel/antiparallel G-quadruplex structure (Figure 30b). In contrast, the two complementary strands remained in B-form duplex conformation, and were not at all affected by the presence of 100 mM KCl.

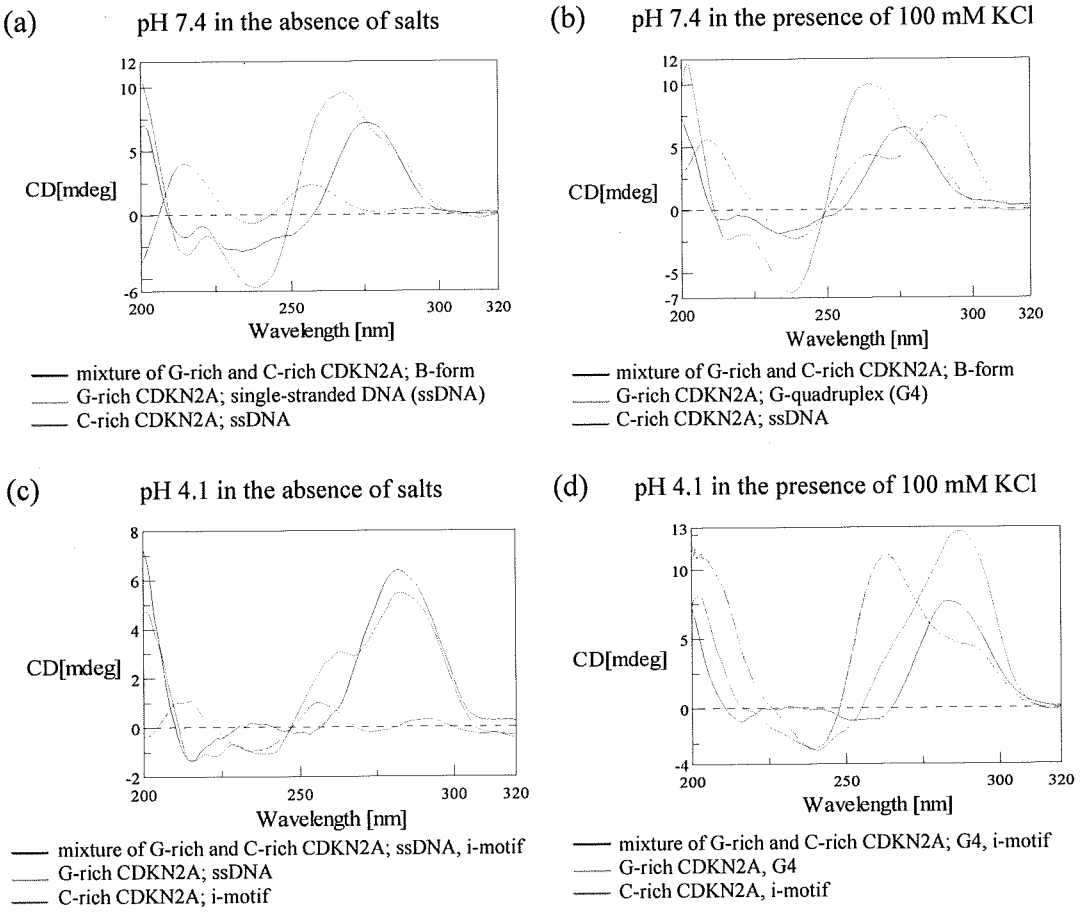

Figure 30 CD spectra of G-rich CDKN2A, C-rich CDKN2A, and the mixture of two complementary strands of CDKN2A under the specified conditions.

To investigate the effects of i-motif formation on the disruption of duplex structures, double-stranded CDKN2A was incubated at pH 4.1 in the absence of salts. The resulting CD spectrum (Figure 30c) showed dramatic changes when compared to those of the B-form conformation. The characteristic broad positive band around 260-280 nm of the B-form conformation became split into two positive peaks with diminished intensity around 260 nm and increased intensity around 280 nm. The arisen peak at 280 nm coincided with that observed with C-rich CDKN2A (Figure 30c, red line). Therefore, this dramatic change in the CD spectrum of double-stranded CDKN2A implied the conversion of the

G-rich strand in the duplex to an i-motif structure. To further confirm this speculation, the melting temperatures of various structures under these conditions were determined, and the results are shown in Figure 31. As compared with the melting curve of duplex CDKN2A at pH 7.4 without salts (Figure 31a), which was obviously monophasic with a melting temperature of 50°C, the double-stranded CDKN2A in the absence of salts at pH 4.1 showed a totally different melting profile (Figure 31b), confirming that duplex CDKN2A could be converted to other structures at a lower pH. Unfortunately, since the melting curve exhibited an unclear pattern, it could not be used to predict a precise meting temperature value. However, the arisen structure might be a mixture of the C-rich strand with an i-motif structure and an unstructured G-rich strand, based on the CD data.

Ultimately, 100 mM KCl at pH 4.1 was used to induce structural conversion. The resulting CD spectrum of double-stranded CDKN2A also showed a dramatic change, consisting of a broad positive peak around 290 nm accompanied by a positive shoulder near 260 nm. The arisen structure of double-stranded CDKN2A under this condition could be a mixture of an i-motif structure adopted by the C-rich strand and a G-quadruplex structure adopted by the G-rich strand. Thus, to prove this assumption, a melting experiment was also constructed. As shown in Figure 31c, the melting curve produced by the double-stranded CDKN2A in the presence of 100 mM KCl at pH 4.1 obviously exhibited a biphasic pattern with two melting temperatures of 24 and 63°C, which are consistent with the T_m values of the i-motif adopted by C-rich CDKN2A (Figure 31e) and the G-quadruplex structure adopted by G-rich CDKN2A (Figure 31d), respectively. Thus, upon lowering the pH to 4.1 in the presence of 100 mM KCl, duplex CDKN2A was converted to i-motif and G-quadruplex structures. As described above, the presence of 100 mM KCl alone could

not induce structural conversion of duplex CDKN2A. In contrast, duplex CDKN2A could be converted to other structures by lowering the pH to 4.1, either with or without 100 mM KCl. Therefore, a plausible mechanism of such induction is that upon lowering the pH, the C-rich strand in the duplex was first converted to an i-motif structure, allowing the G-rich complementary strand to either remain as single-stranded in the absence of salts or form a G-quadruplex structure when induced by 100 mM KCl.

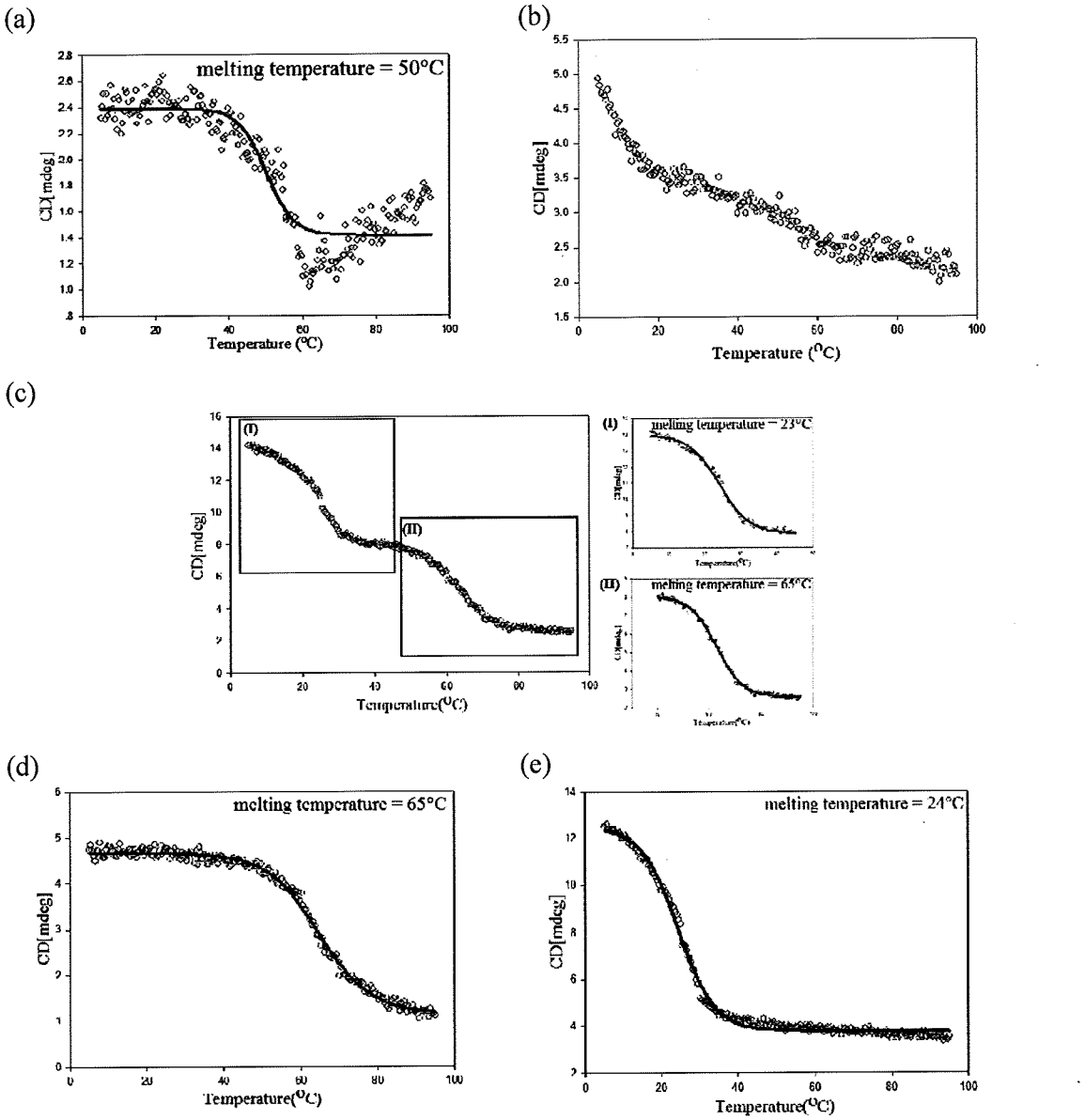

Figure 31 Melting curves of (a) B-form duplex adopted by two complementary strands of CDKN2A in 1XTE (pH 7.4) in the absence of salts, (b) double-stranded CDKN2A in the absence of salts at pH 4.1, (c) double-stranded CDKN2A in the presence of 100 mM KCl at pH 4.1, (d) G-quadruplex structure adopted by G-rich CDKN2A in the presence of 100 mM KCl at pH 4.1, and (e) i-motif structure adopted by C-rich CDKN2A in the absence of salts at pH 4.1.

Conclusion

Herein, we demonstrate that the G-rich sequences in the promoter regions of CDKN2A tumor suppressor gene and NF-ΚB1 proto-oncogene have ability to form stable mixed parallel/antiparallel G-quadruplex structures, as indicated by CD spectroscopy and melting experiments. In addition, a mixed parallel/antiparallel G-quadruplex structure adopted by CDKN2A in the presence of KCl is further characterized by DMS footprinting experiments to reveal that this G-quadruplex structure is comprised of five-base, two-base, and three-base loops. Moreover, the plausible topologies of the mixed parallel/antiparallel G-quadruplex structures are proposed. The stable G-quadruplex structures form within the promoter regions of either NF-ΚB1 proto-oncogene or CDKN2A tumor suppressor gene may play an important biological role in gene regulation by inhibiting their expression.

Therapeutically, stabilization of the formed G-quadruplex structures by small molecules would be beneficial in the case of NF-ΚB1 proto-oncogene to inhibit gene expression, whereas unwinding of those structures would be required in the case of CDKN2A tumor suppressor gene to enhance its expression. Thus, the effects of ligands on these G-quadruplex structures are investigated. We show that two G-quadruplex interacting agents, TMPyP4 and NMM displayed various effects, including induction, destabilization, topological change, on the G-quadruplex structures. In addition, UV-Vis titration experiments use to determine binding parameters (stoichiometry and binding constants) for the interactions between TMPyP4 and the G-quadruplex structures. The results for CDKN2A reveal stoichiometry constants of 1.76 and 1.94 with the apparent binding affinity constants of 2.50 $x10^{9}$ and 2.16$x10^{6}$ M^{-1}, whereas the values for NF-ΚB1 were

1.57 and 3.56 with the apparent binding affinity constants of $1.14x10^{10}$ and $2.81x10^{6}$ M^{-1}. Ultimately, the competition experiments between duplex- and G-quadruplex or i-motif formation of CDKN2A gene suggested that G-quadruplex formation could present under certain conditions, even in the presence of the C-rich complementary strand, which can hybridize with the G-rich strand to form a stable Watson-Crick double helix.

Interestingly, both of the genes focused in this study could adopt mixed parallel/antiparallel G-quadruplex structures with different types of loops compared with those suggested in the literature. For further information, the solution structure of G-quadruplex may be determined to elucidate these loops could result in the formation of mixed parallel/antiparallel G-quadruplex structures. In addition, to design small molecules with high affinity and selectivity to the G-quadruplex structures, the insights on their topologies are essential. Therefore, as a further step, the G-quadruplex structures formed within the promoter regions of both genes should undergo thorough topological characterization of their solution structures by NMR spectroscopy and crystal structures by crystallography.

Reference

1. McEachern, M. J.; Krauskopf, A.; Blackburn, E. H., Telomeres and their control. *Annual review of genetics* **2000,** *34*, 331-358.

2. Sun, D.; Guo, K.; Rusche, J. J.; Hurley, L. H., Facilitation of a structural transition in the polypurine/polypyrimidine tract within the proximal promoter region of the human VEGF gene by the presence of potassium and G-quadruplex-interactive agents. *Nucleic acids research* **2005,** *33* (18), 6070-6080.

3. Rankin, S.; Reszka, A. P.; Huppert, J.; Zloh, M.; Parkinson, G. N.; Todd, A. K.; Ladame, S.; Balasubramanian, S.; Neidle, S., Putative DNA Quadruplex Formation within the Human c-kit Oncogene. *Journal of the American Chemical Society* **2005,** *127* (30), 10584-10589.

4. Eddy, J.; Maizels, N., Gene function correlates with potential for G4 DNA formation in the human genome. *Nucleic acids research* **2006,** *34* (14), 3887-3896.

5. Duquette, M. L.; Huber, M. D.; Maizels, N., G-rich proto-oncogenes are targeted for genomic instability in B-cell lymphomas. *Cancer research* **2007,** *67* (6), 2586-2594.

6. Huppert, J. L.; Balasubramanian, S., Prevalence of quadruplexes in the human genome. *Nucleic acids research* **2005,** *33* (9), 2908-2916.

7. Huppert, J. L.; Balasubramanian, S., G-quadruplexes in promoters throughout the human genome. *Nucleic acids research* **2007,** *35* (2), 406-413.

8. Qin, Y.; Hurley, L. H., Structures, folding patterns, and functions of intramolecular DNA G-quadruplexes found in eukaryotic promoter regions. *Biochimie* **2008,** *90* (8), 1149-1171.

9. Neidle, S., The structures of quadruplex nucleic acids and their drug complexes. *Current opinion in structural biology* **2009,** *19* (3), 239-250.

10. Dingley, A. J.; Peterson, R. D.; Grzesiek, S.; Feigon, J., Characterization of the cation and temperature dependence of DNA quadruplex hydrogen bond properties using high-resolution NMR. *Journal of the American Chemical Society* **2005,** *127* (41), 14466-14472.

11. Burge, S.; Parkinson, G. N.; Hazel, P.; Todd, A. K.; Neidle, S., Quadruplex DNA: sequence, topology and structure. *Nucleic acids research* **2006,** *34* (19), 5402-5415.

12. Kerwin, S. M., G-Quadruplex DNA as a target for drug design. *Current pharmaceutical design* **2000,** *6* (4), 441-478.

13. Shankar, B.; Laurence, H. H.; Stephen, N., Targeting G-quadruplexes in gene promoters: a novel anticancer strategy? *Nature Reviews Drug Discovery* **2011,** *10* (4), 261-275.

14. Falk, J. E., *Porphyrins and metalloporphyrins : their general, physical and coordination chemistry, and laboratory methods*. Elsevier: Amsterdam; London; New York, 1964; Vol. 266.

15. Ren, J.; Qu, X.; Trent, J. O.; Chaires, J. B., Tiny telomere DNA. *Nucleic acids research* **2002,** *30* (11), 2307-2315.

16. Zheng, C.; Yin, Q.; Wu, H., Structural studies of NF-kappaB signaling. *Cell research* **2011,** *21* (1), 183-195.

17. Sun, H.; Bennett, R. J.; Maizels, N., The Saccharomyces cerevisiae Sgs1 helicase efficiently unwinds G-G paired DNAs. *Nucleic acids research* **1999,** *27* (9), 1978-1984.

18. Fry, M.; Loeb, L. A., Human werner syndrome DNA helicase unwinds tetrahelical structures of the fragile X syndrome repeat sequence d(CGG)n. *The Journal of biological chemistry* **1999,** *274* (18), 12797-12802.

19. Patel, D. J.; Phan, A. T.; Kuryavyi, V., Human telomere, oncogenic promoter and 5'-UTR G-quadruplexes: diverse higher order DNA and RNA targets for cancer therapeutics. *Nucleic acids research* **2007,** *35* (22), 7429-7455.

20. Sandell, L. L.; Zakian, V. A., Loss of a yeast telomere: arrest, recovery, and chromosome loss. *Cell* **1993,** *75* (4), 729-739.

21. Siddiqui-Jain, A.; Grand, C. L.; Bearss, D. J.; Hurley, L. H., Direct evidence for a G-quadruplex in a promoter region and its targeting with a small molecule to repress c-MYC transcription. *Proceedings of the National Academy of Sciences of the United States of America* **2002,** *99* (18), 11593-11598.

22. Grand, C. L.; Han, H.; Muñoz, R. M.; Weitman, S.; Von Hoff, D. D.; Hurley, L. H.; Bearss, D. J., The Cationic Porphyrin TMPyP4 Down-Regulates c-MYC and Human

Telomerase Reverse Transcriptase Expression and Inhibits Tumor Growth in Vivo 1 This research was supported by grants from the NIH and the Arizona Disease Control Research Commission.1. *Molecular Cancer Therapeutics* **2002,** *1* (8), 565-573.

23. Watson, J. D.; Crick, F. H. C., Molecular structure of nucleic acids: A structure for deoxyribose nucleic acid. *Nature* **1953,** *171* (4356), 737-738.

24. Halder, K.; Mathur, V.; Chugh, D.; Verma, A.; Chowdhury, S., Quadruplex-duplex competition in the nuclease hypersensitive element of human c-myc promoter: C to T mutation in C-rich strand enhances duplex association. *Biochemical and biophysical research communications* **2005,** *327* (1), 49-56.

25. Bardin, C.; Leroy, J. L., The formation pathway of tetramolecular G-quadruplexes. *Nucleic acids research* **2008,** *36* (2), 477-488.

26. Paramasivan, S.; Rujan, I.; Bolton, P. H., Circular dichroism of quadruplex DNAs: applications to structure, cation effects and ligand binding. *Methods (San Diego, Calif.)* **2007,** *43* (4), 324-331.

27. Karsisiotis, A. I.; Hessari, N. M. a.; Novellino, E.; Spada, G. P.; Randazzo, A.; Webba da Silva, M., Topological Characterization of Nucleic Acid G-Quadruplexes by UV Absorption and Circular Dichroism. *Angewandte Chemie* **2011,** *123* (45), 10833-10836.

28. Membrino, A.; Cogoi, S.; Pedersen, E. B.; Xodo, L. E., G4-DNA Formation in the *HRAS* Promoter and Rational Design of Decoy Oligonucleotides for Cancer Therapy. *PLoS ONE* **2011,** *6* (9), e24421.

29. Cang, X.; Sponer, J.; Cheatham, T. E., 3rd, Explaining the varied glycosidic conformational, G-tract length and sequence preferences for anti-parallel G-quadruplexes. *Nucleic acids research* **2011,** *39* (10), 4499-4512.

30. Hud, N. V.; Smith, F. W.; Anet, F. A.; Feigon, J., The selectivity for K+ versus Na+ in DNA quadruplexes is dominated by relative free energies of hydration: a thermodynamic analysis by 1H NMR. *Biochemistry* **1996,** *35* (48), 15383-15390.

31. Cang, X.; Šponer, J.; Cheatham, I. I. I. T. E., Insight into G-DNA Structural Polymorphism and Folding from Sequence and Loop Connectivity through Free Energy Analysis. *Journal of the American Chemical Society* **2011,** *133* (36), 14270-14279.

32. Sun, D.; Hurley, L. H., Biochemical Techniques for the Characterization of G-Quadruplex Structures: EMSA, DMS Footprinting, and DNA Polymerase Stop Assay. 2008; Vol. 608, pp 65-79.

33. Sun, D.; Hurley, L. H., Biochemical techniques for the characterization of G-quadruplex structures: EMSA, DMS footprinting, and DNA polymerase stop assay. *Methods in molecular biology (Clifton, N.J.)* **2010,** *608*, 65-79.

34. Li, T.; Wang, E.; Dong, S., Parallel G-Quadruplex-Specific Fluorescent Probe for Monitoring DNA Structural Changes and Label-Free Detection of Potassium Ion. *Analytical Chemistry* **2010,** *82* (18), 7576-7580.

35. Nicoludis, J. M.; Barrett, S. P.; Mergny, J. L.; Yatsunyk, L. A., Interaction of human telomeric DNA with N-methyl mesoporphyrin IX. *Nucleic acids research* **2012,** *40* (12), 5432-5447.

36. Gray, R. D.; Li, J.; Chaires, J. B., Energetics and Kinetics of a Conformational Switch in G-Quadruplex DNA†. *The Journal of Physical Chemistry B* **2009,** *113* (9), 2676-2683.

37. Haider, S. M.; Neidle, S.; Parkinson, G. N., A structural analysis of G-quadruplex/ligand interactions. *Biochimie* **2011,** *93* (8), 1239-1251.

38. Wei, C.; Wang, L.; Jia, G.; Zhou, J.; Han, G.; Li, C., The binding mode of porphyrins with cation side arms to (TG4T)4 G-quadruplex: spectroscopic evidence. *Biophysical chemistry* **2009,** *143* (1-2), 79-84.

39. Ambrus, A.; Chen, D.; Dai, J.; Bialis, T.; Jones, R. A.; Yang, D., Human telomeric sequence forms a hybrid-type intramolecular G-quadruplex structure with mixed parallel/antiparallel strands in potassium solution. *Nucleic acids research* **2006,** *34* (9), 2723-2735.

40. Luu, K. N.; Phan, A. T.; Kuryavyi, V.; Lacroix, L.; Patel, D. J., Structure of the human telomere in K+ solution: an intramolecular (3+ 1) G-quadruplex scaffold. *J. Am. Chem. Soc.* **2006,** *128* (30), 9963-9970.

41. Xu, Y.; Noguchi, Y.; Sugiyama, H., The new models of the human telomere d[AGGG(TTAGGG)3] in K+ solution. *Bioorganic & Medicinal Chemistry* **2006,** *14* (16), 5584-5591.

42. Zhang, H. J.; Wang, X. F.; Wang, P.; Ai, X. C.; Zhang, J. P., Spectroscopic study on the binding of a cationic porphyrin to DNA G-quadruplex under different K+ concentrations. *Photochemical & photobiological sciences : Official journal of the European*

Photochemistry Association and the European Society for Photobiology **2008,** *7* (8), 948-955.

43. Pasternack, R. F.; Gibbs, E. J.; Villafranca, J. J., Interactions of porphyrins with nucleic acids. *Biochemistry* **1983,** *22* (23), 5409-5417.

44. Parkinson, G. N.; Ghosh, R.; Neidle, S., Structural basis for binding of porphyrin to human telomeres. *Biochemistry* **2007,** *46* (9), 2390-2397.

45. Phan, A. T.; Kuryavyi, V.; Gaw, H. Y.; Patel, D. J., Small-molecule interaction with a five-guanine-tract G-quadruplex structure from the human MYC promoter. *Nature chemical biology* **2005,** *1* (3), 167-173.

46. Kypr, J.; Kejnovská, I.; RenČiuk, D.; VorlíČková, M., Circular dichroism and conformational polymorphism of DNA. *Nucleic acids research* **2009,** *37* (6), 1713-1725.

Output

In our study, we demonstrate that the G-rich sequences in the promoter regions of CDKN2A tumor suppressor gene and NF-ĸB1 proto-oncogene have ability to form stable mixed parallel/antiparallel G-quadruplex structures. The mixed parallel/antiparallel G-quadruplex structure from CDKN2A is comprised of five-base, two-base, and three-base loops adopted by CDKN2A in the presence of KCl. The stable G-quadruplex structures form within the promoter regions of either NF-ĸB1 proto-oncogene or CDKN2A tumor suppressor gene may play an important biological role in gene regulation.

Moreover, we show that two G-quadruplex interacting agents, TMPyP4 and NMM displayed various effects, including induction, destabilization, topological change, on the G-quadruplex structures. The results for CDKN2A reveal stoichiometry constants of 1.76 and 1.94 with the apparent binding affinity constants of 2.50 $x10^{9}$ and $2.16x10^{6}$ M^{-1}, whereas the values for NF-ĸB1 were 1.57 and 3.56 with the apparent binding affinity constants of $1.14x10^{10}$ and $2.81x10^{6}$ M^{-1}. Ultimately, the competition experiments between duplex- and G-quadruplex or i-motif formation of CDKN2A gene suggested that G-quadruplex formation could present under certain conditions, even in the presence of the C-rich complementary strand, which can hybridize with the G-rich strand to form a stable Watson-Crick double helix.

Appendix

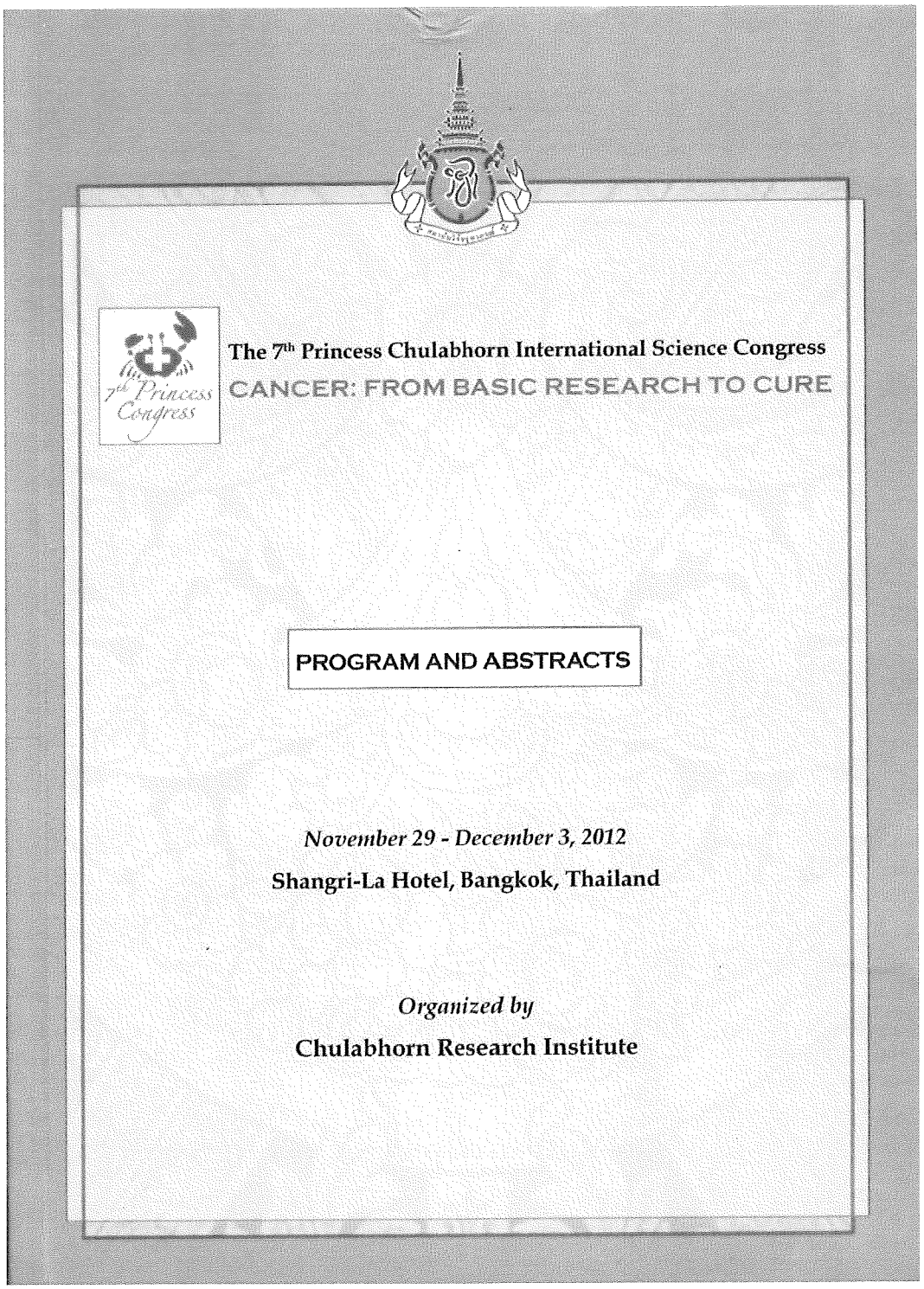
The 7th Princess Chulabhorn International Science Congress
CANCER: FROM BASIC RESEARCH TO CURE
PROGRAM AND ABSTRACTS
November 29 - December 3, 2012
Shangri-La Hotel, Bangkok, Thailand
Organized by
Chulabhorn Research Institute

The 7th Princess Chulabhorn International Science Congress

CANCER: FROM BASIC RESEARCH TO CURE

November 29 - December 3, 2012

Shangri-La Hotel, Bangkok, Thailand

Published by: Ink On Paper Company Limited, Bangkok, Thailand

ISBN: 978-974-7408-17-1

SCIENTIFIC PROGRAM

OPENING SESSION

Thursday, November 29, 2012

OPENING CEREMONY

Time	*Grand Ballroom, Shangri-La Hotel*	
15:45	- Guests to be seated in the Ballroom	
16:00	- Arrival of Professor Dr. HRH Princess Chulabhorn - Video presentation in honor of the celebrations of 84 years of the birth of His Majesty King Bhumibol and 80 years of the birth of Her Majesty Queen Sirikit	
16:10	- Report by Dr. *Khunying* Mathuros Ruchirawat, Secretary General of the National Organizing Committee	
16:15	- Opening address by Professor Dr. HRH Princess Chulabhorn	
16:20	- Keynote address: "Environment and life-style factors contributing to cancer incidence in Asia" by Professor Dr. HRH Princess Chulabhorn Introduced by Professor Gerald N. Wogan	***Abstract No.*** KA
17:30	**CONGRESS DINNER** ***at Royal Thai Navy Convention Hall*** Leave Shangri-La Hotel by boat	

SCIENTIFIC PROGRAM

SUMMARY

Friday, November 30, 2012

Time	Ballroom I, II, III	Abstract No.
09:00	**NOBEL LAUREATE LECTURE:** **Chairpersons:** Mahidol, C. (THAILAND) and Wiltrout, R.H. (U.S.A.) Nobel Laureate Lecture: Cancer: The genomic era arrives *Bishop, J.M. (Nobel Laureate, U.S.A.)*	NL

	PLENARY LECTURES:	Abstract No.	Myanmar Room at Krungthep Wing
09:45	Plenary Lecture 1: Molecular epidemiology: Cancer etiology and prevention *Wild, C.P. (IARC, FRANCE)*	PL-1	**CLINICAL RESEARCH SYMPOSIUM:**
10:30	Plenary Lecture 2: Environmental and occupational determinants of cancer: interventions for primary prevention *Neira, M.P. (WHO, GENEVA)*	PL-2	10:30 **Advances in Epidemiology and Imaging of Cancers** **Chairpersons:** Suwanwela, C. (THAILAND) Pattaranutaporn, P. (THAILAND)
11:15	Plenary Lecture 3: Public health aspects of cancer *Pilanbangchang, S. (WHO, SEARO)*	PL-3	**Abstract No.** Advances in epidemiologic studies of cancer C-1 *Boffetta, P. (U.S.A.)* Advances in molecular imaging of cancer C-2 *Israel, O. (ISRAEL)*
12:00	L U N C H		

POSTER PRESENTATION:

PA-01 to PC-12

Display: November 30, 09:00 to December 1, 14:00

Discussion: November 30 and December 1, 12:30-14:00

Time	Ballroom I	Ballroom II	Ballroom III	L U N C H
14:00	**SYMPOSIUM I:** **Cancer Etiology, Mechanisms and Epigenetics** **Chairpersons:** Trosko, J.E. (U.S.A.) Mongkolsuk, S. (THAILAND) **Abstract No.** Dormant blood stem cells and circulating cancer stem cells S-1 *Trumpp, A. (GERMANY)* Modulation of adult stem cells *in utero* by diet and environmental chemicals alters risks to cancer later in life: A possible mechanism of the Barker hypothesis S-2 *Trosko, J.E. (U.S.A.)* Epigenetics and cancer: New opportunities and challenges S-3 *Herceg, Z. (IARC, FRANCE)* Genomic instability and gene regulation mechanisms in cis of DNA hypomethylation in human cancer S-4 *Mutirangura, A. (THAILAND)* Proteomic analyses of the core cell cycle machinery in human cancer cells S-5 *Sicinski, P. (U.S.A.)*	**SYMPOSIUM II:** **Carcinogenesis: Environment and Emerging Exposures** **Chairpersons:** Shank, R.C. (U.S.A.) Autrup, H.N. (DENMARK) **Abstract No.** Ambient air pollution and cancer risk S-6 *Autrup, H.N. (DENMARK)* Windows of susceptibility: Environmental exposures in the etiology of breast cancer S-7 *Colman, G.W. (U.S.A.)* Naturally occurring and process-generated carcinogens in food S-8 *Schrenk, D. (GERMANY)* Cancer risk and the nuclear disaster in Japan S-9 *Kanno, J. (JAPAN)* Childhood leukaemia and EMFs: Mobile phones and brain tumours, risks and causal pathways S-10 *Henshaw, D.L. (U.K.)* Infection, environmental exposure and cancer S-11 *Anwar, W.A. (EGYPT)*	**SYMPOSIUM III:** **Approaches to Early Detection and Diagnosis** **Chairpersons:** Gascoyne, P.R.C. (U.S.A.) Frank, N. (GERMANY) **Abstract No.** Antibody-independent isolation of circulating cancer cells by dielectrophoretic fractionation S-12 *Gascoyne, P.R.C. (U.S.A.)* Albumin-drug conjugates: "Magic bullets" in cancer therapy and diagnosis S-13 *Frei, E. (GERMANY)* 4DPET-CT for tumor diagnostics and therapy management: A new approach to gain noninvasively molecular biological data in patients S-14 *Strauss, L.G. (GERMANY)* Searching for novel anti-cancer agents and biomarkers using cancer cell lines S-15 *Svasti, J. (THAILAND)* Detection and evaluation of DNA damage in various occupations exposed to different chemicals in Turkey S-15a *Şardaş, S. (TURKEY)*	13:00 **Symposium on Clinical Approaches to Liver Cancers** **Chairpersons:** Pattaranutaporn, P. (THAILAND) Auewarakul, C.U. (THAILAND) **Abstract No.** Epidemiology of liver cancer C-3 *Boffetta, P. (U.S.A.)* Diagnostic imaging of primary liver cancer C-4 *Israel, O. (ISRAEL)* Medical management of hepatocellular carcinoma C-5 *Tanwandee, T. (THAILAND)* Surgical treatment for liver cancer C-6 *Fong, Y. (U.S.A.)* The emerging role of radiotherapy in the management of primary and metastatic liver cancer C-7 *Kuten, A. (ISRAEL)* Molecular targeted therapy in hepatocellular carcinoma C-8 *Sriuranpong, V. (THAILAND)*

PROGRAM SUMMARY

Saturday, December 1, 2012

Time	Ballroom I, II, III
	PLENARY LECTURES: **Abstract No.** **Chairpersons:** Wogan, G.N. (U.S.A.) and Ruchirawat, M. (THAILAND)
09:00	Plenary Lecture 4: Recognition of 'foreign' antigens by the immune system **PL-4** *Wilson, I.A. (U.S.A.)*
09:50	Plenary Lecture 5: Inflammation and cancer: Interweaving microRNA, free radicals, cytokine and p53 pathways **PL-5** *Harris, C.C. (U.S.A.)*
10:40	Plenary Lecture 6: Understanding early life exposures in childhood and adult cancers **PL-6** *Suk, W.A. (U.S.A.)*
11:30	*L U N C H*

POSTER PRESENTATION:

PA-01 to PC-12

Display: November 30, 09:00 to December 1, 14:00

Discussion: November 30 and December 1, 12:30-14:00

PD-01 to PG-45

Display: December 1, 14:30 to December 2, 17:30

Discussion: December 2, 12:00-14:00 and 17:00-17:30

Time	Ballroom I	Ballroom II	Ballroom III
14:00	***SYMPOSIUM IV:*** ***Recent Advances in Liver Cancer Research*** **Chairpersons:** Harris, C.C. (U.S.A.) Wang, X.W. (U.S.A.) **Abstract No.** Oncogene-driven mouse liver cancers can be differentially influenced by immune mechanisms **S-16** *Wiltrout, R.H. (U.S.A.)* Liver cancer stem cells in hepatocellular carcinoma **S-17** *Ng, I.O.L. (HONG KONG)* Defining liver cancer heterogeneity, tumor subtypes and cancer stem cells **S-18** *Wang, X.W. (U.S.A.)* Predictive power of hepatitis B mutations in plasma for detection and risk of hepatocellular carcinoma **S-19** *Groopman, J.D. (U.S.A.)* Community-based prevention of liver cancer **S-20** *Loffredo, C.A. (U.S.A.)*	***SYMPOSIUM V:*** ***Fetal Origins of Cancer*** **Chairpersons:** Buffler, P.A. (U.S.A.) Suk, W.A. (U.S.A.) **Abstract No.** Early life exposures and childhood cancer: Epidemiologic observations **S-21** *Buffler, P.A. (U.S.A.)* Tumor genetic, epigenetic and immune clues of the fetal origin of childhood leukemia **S-22** *Wiemels, J.L. (U.S.A.)* Humans under double attack. Gut microbiota composition, and postnatal fluctuations in body burdens of environmental toxicants, are both exposures that need more consideration **S-23** *Eggesbø, M. (NORWAY)* Newborns and genotoxic risks: A summary of the NewGeneris project **S-24** *Kleinjans, J. (THE NETHERLANDS)*	***SYMPOSIUM VI:*** ***New Approaches Towards Individualized Cancer Therapeutics*** **Chairpersons:** Mihich, E. (U.S.A.) Zänker, K.S. (GERMANY) **Abstract No.** Functional genomics *en route* to novel target identification in personalized cancer theranostics **S-25** *Rossbach, M. (SINGAPORE)* The transcription factor PITX2 (pituitary homeobox 2) protects renal cancer cell lines against doxorubicin toxicity by trans-activation of the multidrug transporter ABCB1 **S-26** *Thévenod, F. (GERMANY)* MicroRNAs in cancer **S-27** *Novina, C.D. (U.S.A.)* Patient characterization in early clinical trials **S-28** *Banerji, U. (U.K.)* Detection of minimal residual disease in acute myeloid leukemia – A model for individualized cancer therapy **S-29** *Hokland, P. (DENMARK)* Adrenergic receptor targeted therapy: From the bench towards personalized treatment in oncology **S-30** *Zänker, K.S. (GERMANY)* Concluding remarks *Zänker, K.S. (GERMANY)*

PROGRAM SUMMARY

Sunday, December 2, 2012

Time	Ballroom I, II, III
	PLENARY LECTURES: — Abstract No.
	Chairpersons: Groopman, J. (U.S.A.) and Svasti, J. (THAILAND)
09:00	Plenary Lecture 7: New medicines for cancer arising from surprising new biology — *Schimmel, P. (U.S.A.)* — PL-7
09:50	Plenary Lecture 8: The role of obesity, physical activity and metabolic factors in cancer aetiology — *Riboli, E. (U.K.)* — PL-8
10:40	Plenary Lecture 9: Molecular targets for cancer chemoprevention — *Steele, V.E. (U.S.A.)* — PL-9
11:30	L U N C H

POSTER PRESENTATION:
PD-01 to PG-45
Display: December 1, 14:30 to December 2, 17:30
Discussion: December 2, 12:00-14:00 and 17:00-17:30

Time	Ballroom I	Ballroom II	Ballroom III
14:00	***SYMPOSIUM VII:*** ***Arsenic: Complex Environmental Contaminant Linked to Cancer and Other Chronic Diseases*** **Chairpersons:** Suk, W.A. (U.S.A.) Fry, R.C. (U.S.A.)	***SYMPOSIUM VIII:*** ***Drug Discoveries*** **Chairpersons:** Siegel, J. (SWITZERLAND) Ruchirawat, S. (THAILAND)	***SYMPOSIUM IX:*** ***Novel Approaches to the Treatment of Cancer*** **Chairpersons:** Feun, L.G. (U.S.A.) Auewarakul, C.U. (THAILAND)
		Abstract No.	***Abstract No.***
	Health risk assessment of arsenic exposure through groundwater drinking pathway in Southeast Asia — *Kim, K-W. (KOREA)* — S-31	Natural products from multiple sources as leads to anticancer drugs — *Newman, D.J. (U.S.A.)* — S-38	Therapeutic strategies targeting ERBB2 — *Pegram, M.D. (U.S.A.)* — S-43
	Arsenic and the epigenome: inter-individual differences in urinary arsenic profiles associated with distinct DNA methylation patterns — *Fry, R.C. (U.S.A.)* — S-32	Seaweed fucoidans - A platform for new drug discovery — *Nifantiev, N.E. (RUSSIA)* — S-39	Novel therapy for non-small cell lung cancer in the 21st century — *Nguyen, D.M. (U.S.A.)* — S-44
	Prenatal to early childhood arsenic exposure: Gene expression, DNA methylation and DNA repair — *Ruchirawat, M. and Navasumrit, P. (THAILAND)* — S-33	Peptidomimetics, protein-protein interactions, and tumor targeting — *Burgess, K. (U.S.A.)* — S-40	Novel therapy for hepatocellular carcinoma — *Feun, L.G. (U.S.A.)* — S-45
	Stem cells in arsenic-induced transplacental carcinogenesis — *Tokar, E.J. (U.S.A.)* — S-34	Recent advances in the chemistry and biology of bioactive natural products — *Chen, D. (SOUTH KOREA)* — S-41	National Cancer Institute's approaches to early experimental therapeutics — *Ivy, S.P. (U.S.A.)* — S-46
	Effect of arsenic on genomic and non-genomic estrogen signalings — *Thiantanawat, A. (THAILAND)* — S-35	Glycomics as key targets for therapeutic intervention — *Shriver, Z.H. (U.S.A.)* — S-42	
	Consequences of arsenic exposure in children — *Graziano, J.H. (U.S.A.)* — S-36		
	Mortality risks from arsenic in drinking water: Impact of exposure on chronic disease — *Smith, A.H. (U.S.A.)* — S-37		

PROGRAM SUMMARY

Monday, December 3, 2012

Time	Ballroom I	Ballroom II	Ballroom III
9:00	***SYMPOSIUM X:*** ***Molecular Approaches and Targets for Cancer Therapy and Prevention*** **Chairpersons:** Samson, L.D. (U.S.A.) Satayavivad, J. (THAILAND) ***Abstract No.*** Eradicating cancer in our lifetime: Novel approaches and new horizons S-47 *Chakrabarty, A.M. (U.S.A.)* Application of risk factor knowledge to the intervention of cervical cancer S-48 *Au, W.W. (P.R. CHINA)* Chronic inflammation increases cancer risks: Role of reactive nitrogen and oxygen species S-49 *Wogan, G.N. (U.S.A.)* DNA repair is indispensable for survival after acute inflammation in mice S-50 *Samson, L.D. (U.S.A.)* The O^6-alkylguanine response: Implications for cancer therapy S-51 *Kaina, B. (GERMANY)* Molecular target-based chemoprevention of inflammation-associated cancer with edible phytochemicals S-52 *Surh, Y-J. (SOUTH KOREA)*	***SYMPOSIUM XI:*** ***Collegium Ramazzini's Symposium on Hot Topics on Environmental and Occupational Origins of Cancer*** **Moderators:** Mehlman, M.A. (U.S.A.) Soffritti, M. (ITALY) ***Abstract No.*** The IARC monographs programme: Recent evaluations of occupational and environmental carcinogens S-53 *Straif, K. (IARC, FRANCE)* Cancer prevention and control in high risk populations S-54 *Ringen, K. (U.S.A.)* The carcinogenicity of aspartame administered with the feed to rats and mice for the life span S-55 *Soffritti, M. (ITALY)* Chromosome 5 and 7 abnormalities in oncology personnel handling anti-cancer drugs S-56 *McDiarmid, M. (U.S.A.)* Salivary biomarkers of environmental cancer S-57 *Koh, D.S.Q. (BRUNEI DARUSSALAM)* Chromosome damage and the damage repair capacity in Chinese VCM-exposed workers S-58 *Xia, Z-L. (P.R. CHINA)*	***SYMPOSIUM XII:*** ***Towards the Cure: Targets for Therapeutic Intervention*** **Chairpersons:** Savaraj, N. (U.S.A.) Ratanabanangkoon, K. (THAILAND) ***Abstract No.*** *In vitro* and *in vivo* investigations of targeted drug delivery to tumor cells using nanoparticles transported by natural carriers (red blood cells) S-59 *Bäumler, H.H. (GERMANY)* Nanopharmaceuticals: Exciting approach for cancer treatment and cure S-60 *Fetzer, O. (U.S.A.)* Targeting tumor metabolism: Back to the future S-61 *Savaraj, N. (U.S.A.)* Targeting ROS and tumor metabolism to kill cisplatin resistant lung cancer S-62 *Wangpaichitr, M. (U.S.A.)* Towards the cure: analysis and intervention in cancer cell chemoresistance S-63 *Gant, T.W. (U.K.)* Autophagy as a target for cancer therapy S-64 *Isidoro, C. (ITALY)*
12:00	*L U N C H*		
Time			***Ballroom I, II, III***
13:30	***CLOSING SESSION:*** ***Challenges and Opportunities: Cancer Treatment from Bench to Bedside*** **Moderator:** Sasisekharan, R. (U.S.A.) **Panelists:** • Rosenblatt, M. (U.S.A.) • Roychowdhury, D. (U.S.A.) • Kania, E.M., Jr. (U.S.A.)		
	CLOSING CEREMONY		***Abstract No.***
15:30	Closing Lecture: Future practice of medicine *Ausiello, D.A. (U.S.A.)*		CL
16:15	• **Signing of Collaboration Agreement between Chulabhorn Research Institute and Center for Cancer Research, National Cancer Institute, U.S.A. - "Thailand's Initiative in Genomics and Expression Research for Liver Cancer (TIGER-LC)"**		
16:25	• **Presentation of the Princess Chulabhorn Gold Medal Award**		
16:40	• **Closing Remarks by Professor Dr. HRH Princess Chulabhorn**		

PG-23

G-QUADRUPLEX MOTIF WITHIN THE PROMOTER REGION OF CDKN2A TUMOR SUPPRESSOR GENE

Parichart Kedkum[1],Montakarn Chittchang[1,2], Bodin Tuesuwan[3]

[1]Chemical Biology Program, Chulabhorn Graduate Institute, and the Center of Excellence on Environment Health and Toxicology under the Science & Technology Postgraduate Education and Research Development Office (PERDO) of the Commission on Higher Education (CHE), Ministry of Education, Bangkok, Thailand, [2]Laboratory of Medicinal Chemistry, Chulabhorn Research Institute, Bangkok, Thailand, [3]Department of Food and Pharmaceutical Chemistry, Faculty of Pharmaceutical Sciences, Chulalongkorn University, Bangkok, Thailand

The promoter region of CDKN2A tumor suppressor gene contains a guanine (G)-rich sequence (5'-GGGCAGCTG GGAGGG GAATGG G-3') with high propensity to form G-quadruplex structures, which may play an important biological role in gene regulation and expression. Thus, G-quadruplex motif within the promoter region of this gene may represent a potential target for anti-cancer drug design.To provide the evidence for the formation of G-quadruplex structures, circular dichroism (CD) spectroscopy and melting experiments were conducted to demonstrate the formation of a stable mixed parallel/antiparallel G-quadruplex structure. Moreover, the G-quadruplex structure adopted in the presence of 100 mM KCl was further characterized by DMS footprinting experiments to reveal a G-quadruplex structure containing three tetrads. In addition, the competition experiments between duplex and G-quadruplex or i-motif formation suggested that G-quadruplex structures could be formed under specified conditions, even in the presence of the C-rich complementary strand.Ultimately, various distinct effects, including induction, destabilization, and topological change, were observed with 5,10,15,20-tetrakis(N-methylpyridinium-4-yl)-21H,23H-porphyrin (TMPyP4) and N-methyl mesoporphyrin (NMM) by using CD spectroscopy. These results provide the evidence for G-quadruplex formation within the promoter region of CDKN2A tumor suppressor gene *in vitro*, which could potentially play a role as a transcriptional regulator of this gene, and could also be manipulated by small molecules.

PG-24

SEMI-SYNTHESIS AND CYTOTOXIC ACTIVITY OF 14-DEOXY-12-HYDROXY-ANDROGRAPHOLIDE DERIVATIVES

Sakkasem Kasemsook[1], Uthaiwan Sirion[1], Kanoknetr Suksen[2], Pawinee Piyachaturawat[2], Apichart Suksamrarn[3], Rungnapha Saeeng[1]

[1]Department of Chemistry and Center for Innovation in Chemistry, Faculty of Science, Burapha University, Chonburi 20131, Thailand, [2]Department of Physiology, Mahidol University, Bangkok 10400, Thailand, [3]Department of Chemistry, Faculty of Science, Ramkhamhaeng University, Bangkok 10240, Thailand

Andrographolide is a major component isolated from Andrographis paniculata and has been shown to exhibit a wide range of pharmacological activities including anticancer activity. In the present study, a series of 14-deoxy-12-hydroxy-andrographolide derivatives has been synthesized from naturally occurring andrographolide by rearrangement reaction with PDC followed by modification of three hydroxyl groups. Fifteen andrographolide derivatives were obtained in good yields and the cytotoxicity of all analogues was evaluated against six cancer cell lines. The results revealed that the conversion of hydroxyl group at C-19 of 14-deoxy-12-hydroxy-andrographolide to trityl- or silyl-ether enhanced the cytotoxic activity. These synthetic compounds were found to potent against ASK cancer cell than the reference drug ellipticin and could be simply obtained under mild condition. These new synthetic compounds may serve as a potential leads for the development of new anticancer drugs.